Article

Structure of the mitochondrial import gate reveals distinct preprotein paths

Yuhei Araiso[1,2,12], Akihisa Tsutsumi[3], Jian Qiu[4,5,13], Kenichiro Imai[6], Takuya Shiota[7,8], Jiyao Song[4], Caroline Lindau[4,9], Lena-Sophie Wenz[4,14], Haruka Sakaue[1,2], Kaori Yunoki[1], Shin Kawano[1,2], Junko Suzuki[1], Marilena Wischnewski[4,15], Conny Schütze[4], Hirotaka Ariyama[10], Toshio Ando[10], Thomas Becker[4,11], Trevor Lithgow[7], Nils Wiedemann[4,11], Nikolaus Pfanner[4,11], Masahide Kikkawa[3] & Toshiya Endo[1,2*]

The translocase of the outer mitochondrial membrane (TOM) is the main entry gate for proteins[1–4]. Here we use cryo-electron microscopy to report the structure of the yeast TOM core complex[5–9] at 3.8-Å resolution. The structure reveals the high-resolution architecture of the translocator consisting of two Tom40 β-barrel channels and α-helical transmembrane subunits, providing insight into critical features that are conserved in all eukaryotes[1–3]. Each Tom40 β-barrel is surrounded by small TOM subunits, and tethered by two Tom22 subunits and one phospholipid. The N-terminal extension of Tom40 forms a helix inside the channel; mutational analysis reveals its dual role in early and late steps in the biogenesis of intermembrane-space proteins in cooperation with Tom5. Each Tom40 channel possesses two precursor exit sites. Tom22, Tom40 and Tom7 guide presequence-containing preproteins to the exit in the middle of the dimer, whereas Tom5 and the Tom40 N extension guide preproteins lacking a presequence to the exit at the periphery of the dimer.

Mitochondria have central roles in cellular energy production, metabolic pathways, lipid biogenesis, signalling and programmed cell death. Mitochondrial functions rely on the assembly of around 1,000 resident proteins, 99% of which are synthesized as preproteins in the cytosol and imported into mitochondria by translocator complexes[1–3]. The TOM complex functions as the main entry gate for more than 90% of mitochondrial proteins. The import pathway then branches into different sorting pathways to the outer membrane, intermembrane space (IMS), inner membrane and matrix, depending on the class of preproteins. In yeast, as in humans, the TOM complex consists of the channel-forming β-barrel protein Tom40 and six α-helical membrane-integrated subunits: the receptors Tom20, Tom22 and Tom70, and regulators Tom5, Tom6 and Tom7. The TOM complex has been observed in three-channel (trimer) and two-channel (dimer) forms[4–9] (Extended Data Fig. 1a).

Preprotein translocation across membranes requires high fidelity for both substrate recognition and substrate movement through a proteinaceous channel. Protein secretion in the bacterial inner membrane and eukaryotic endoplasmic reticulum is driven by a translocon (the SecYEG or Sec61 complex) composed primarily of α-helical membrane-spanning segments[10–14]. Through coordinated movement of the helical segments relative to each other, substrate proteins can be translocated across the membrane or laterally gated into the membrane, depending on their intrinsically determined route through the translocon[10–14]. In the bacterial outer membrane, three protein translocases comprising a β-barrel channel are used either for protein translocation across the membrane (FhaC[15]) or lateral transfer into the membrane (BamA[16] and TamA[17]). The TOM complex represents a fundamentally distinct form of translocator (α/β translocator), composed of a β-barrel channel together with α-helical subunits that coordinate its activity through interactions in the plane of the membrane. To date, the structural information available regarding this complex comes from in situ crosslinking of the trimer[4] and a 6.8-Å medium-resolution cryo-electron microscopy (cryo-EM) structure of the dimer[9]. To understand the architecture and function of the TOM complex, we combined high-resolution cryo-EM and functional analyses. The results reveal how the TOM complex facilitates transport of around 1,000 different preproteins with divergent structural and chemical properties into mitochondria.

Structure of the TOM core complex

We purified the TOM complex from the yeast *Saccharomyces cerevisiae* (Extended Data Fig. 1b–e). The purified TOM complex is a mixture of trimers and dimers[8] (Extended Data Fig. 1a). High-speed atomic force microscopy (HS-AFM) analysis showed that the trimer could be

[1]Faculty of Life Sciences, Kyoto Sangyo University, Kyoto, Japan. [2]Institute for Protein Dynamics, Kyoto Sangyo University, Kyoto, Japan. [3]Department of Cell Biology and Anatomy, Graduate School of Medicine, The University of Tokyo, Tokyo, Japan. [4]Institute of Biochemistry and Molecular Biology, ZBMZ, Faculty of Medicine, University of Freiburg, Freiburg, Germany. [5]Spemann Graduate School of Biology and Medicine, University of Freiburg, Freiburg, Germany. [6]Molecular Profiling Research Center for Drug Discovery (molprof), National Institute of Advanced Industrial Science and Technology (AIST), Tokyo, Japan. [7]Infection and Immunity Program, Biomedicine Discovery Institute and Department of Microbiology, Monash University, Melbourne, Victoria, Australia. [8]Organization for Promotion of Tenure Track, University of Miyazaki, Miyazaki, Japan. [9]Faculty of Biology, University of Freiburg, Freiburg, Germany. [10]Nano Life Science Institute (WPI-Nano LSI), Kanazawa University, Kanazawa, Japan. [11]CIBSS Centre for Integrative Biological Signalling Studies, University of Freiburg, Freiburg, Germany. [12]Present address: Department of Clinical Laboratory Science, Division of Health Sciences, Graduate School of Medical Science, Kanazawa University, Kanazawa, Japan. [13]Present address: Institute of Molecular Precision Medicine and Hunan Key Laboratory of Molecular Precision Medicine, Xiangya Hospital, Central South University, Changsha, China. [14]Present address: Sanofi Deutschland, Frankfurt am Main, Germany. [15]Present address: Swiss Federal Institute of Technology (EPFL), Lausanne, Switzerland. *e-mail: tendo@cc.kyoto-su.ac.jp
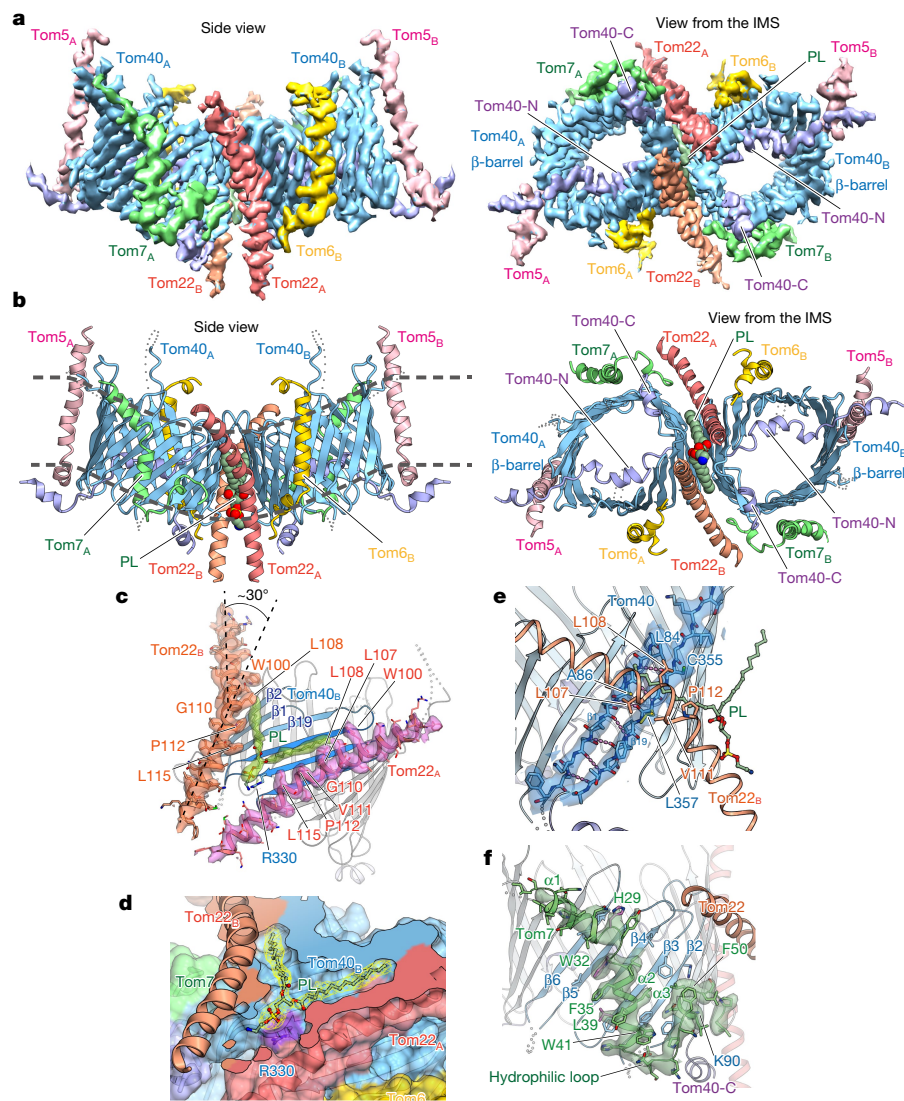
Fig. 1 | Overall structure of the TOM complex and bound phospholipid.
a, **b**, Cryo-EM density of the TOM complex dimer (**a**) and its cartoon representation (**b**). Each subunit is shown in a different colour. The TOM-bound phospholipid (PL), modelled as phosphatidylethanolamine, is shown as a space-filling model. The broken lines (**b**, left panel) indicate the membrane–water interface, which was estimated from the positions of the transmembrane segments for Tom22[34], Tom5, Tom6 and Tom7 calculated by the TMpred server (https://embnet.vital-it.ch/software/TMPRED_form.html). **c**, Close-up view of the two Tom22 molecules and bound phospholipid. Tom22 (cartoon

representation) and PL (space-filling model) are superimposed according to the EM density. **d**, The cavity formed by Tom40 and Tom22 for binding of the phospholipid. Tom40 is shown by cutaway representation. **e**, The association of the first and last β-strands of Tom40 (blue, the EM density is superimposed) is stabilized by Tom22 (red) and phospholipid (green). The head group of the phospholipid was not visible, except for the phosphate, but phosphatidylethanolamine was modelled on the basis of previously reported biochemical results[46]. **f**, Association of Tom7 (green, the EM density is superimposed) with the outer wall of the Tom40 β-barrel.

converted to the dimer (Extended Data Fig. 1f, Supplementary Videos 1, 2). The cryo-EM structure was determined at an effective overall resolution of 3.8 Å as determined by Fourier shell correlation (FSC) (local resolution varying from 3.6 to 5.7 Å) (Fig. 1a, b, Extended Data Fig. 2, Extended Data Table 1). Main chains and many bulky side chains of each subunit were built from the electron microscopy density map or Coulomb potential map and, with the exception of disordered N- or C-terminal segments and short loops, the main chains were visualized as continuous density. The structure showed two molecules each of Tom40, Tom22, Tom5, Tom6 and Tom7, with a two-fold symmetry and dimensions of 66 Å × 48 Å × 65 Å for each protomer, corresponding to the previously observed TOM core complex[7–9] (Extended Data Fig. 1a). Initially, the purified TOM complex fraction contained the receptor Tom20 (Extended Data Fig. 1d), but the association of Tom20 with the TOM core complex is labile, and thus the stable particles used

for determination of the dimeric structure lacked Tom20, consistent with the reported increased stability of the dimeric form in the absence of Tom20[7,8,18]. The channel subunit Tom40 forms a 19-stranded transmembrane β-barrel, with β-strand lengths varying from 5 to 12 residues (Extended Data Fig. 3a). The Tom22, Tom5, Tom6 and Tom7 transmembrane α-helices are closely apposed to the β-barrel (Extended Data Fig. 3b).

α–β contacts and lipid in the dimer

Comparative sequence analysis suggested the evolution of the TOM complex from an ancestral complex consisting of Tom40, Tom22 and Tom7[19,20]. Bioinformatics assessment of Tom7 homologues from the broad range of eukaryotic lineages revealed a universal code of aromatic and hydrophilic residues stamped in its predicted transmembrane

segment[21]. The universally conserved glycine and proline residues (P34, G40 and P48 in the yeast protein) of Tom7 were a particularly distinct feature, given that proline is rarely found in transmembrane segments[22]. Proline residues are also found universally in the transmembrane segment of Tom22 at a conserved position with respect to the *cis* membrane surface, corresponding to P112 in the yeast protein[21]. Consistent with these conserved, helix-breaking residues, a distinct feature of the TOM complex is the arrangement of noticeably kinked transmembrane α-helices of Tom7 and Tom22 around the two Tom40 β-barrels (Fig. 1a, b).

The two Tom40 β-barrels are tethered by the two molecules of Tom22 inserted between them. Tom22 forms a continuously apposed transmembrane α-helix, kinked by 30° through G110 and P112 (Fig. 1c) to follow the contour of the Tom40 β-barrel. The α–β contacts between Tom40 and Tom22 are largely mediated through hydrophobic residues (Fig. 1c). The IMS or C-terminal halves of the kinked Tom22 helices run in parallel between the Tom40 β-barrel dimer, keeping the β-barrels apart. The IMS halves of the Tom22 helices and the Tom40 β-barrels form an intramembrane cavity at the dimer interface, in which a phospholipid molecule was observed, with its head group facing the IMS (Fig. 1c, d). The acidic phosphate group was located close to the conserved R330 of Tom40. The cytosolic halves of the Tom22 helices run outward from the β-barrel dimer interface, and the acyl chains of the phospholipid are held in the resultant space between the Tom40 β-barrels in the vicinity of hydrophobic residues (Fig. 1b). The Tom40 β-barrels directly contact each other near the membrane–cytosol interface. The insertion of the IMS halves of the kinked Tom22 helices together with the phospholipid head group between the IMS side of the Tom40 protomers provides a structural explanation for the observed tilt[9] of the Tom40 β-barrels relative to each other (Fig. 1a, b, side views), which probably distorts the lipid bilayer.

The first (β1) and last (β19) β-strands of Tom40 associate to stably close the β-barrel with seven hydrogen bonds (Extended Data Fig. 3a). The structure of the Tom40 β-barrel is further stabilized by association of the two Tom22 transmembrane helices and the acyl chains of the bound phospholipid (Fig. 1e, Extended Data Fig. 3b). The Tom40 β-barrel could potentially undergo a lateral opening for insertion of outer-membrane proteins[23] analogous to the bacterial system of BamA[17] and TamA[16], and Sam50 (also known as Tob55) of the mitochondrial sorting and assembly machinery[24]. This lateral gating of Tom40 would require Tom22 to shift sideways, a dynamic movement previously envisaged in the TOM complex dimer–trimer transition in intact mitochondria[4,5] (Extended Data Fig. 1a).

Tom7 has a highly unusual membrane topology in which a short hydrophobic helix, α2, spans the membrane core, presents a subsequent hydrophilic segment to the IMS side of the membrane and then diverts back into the lipid core by forming a short C-terminal hydrophobic helix α3. This topology traverses six Tom40 β-strands (Fig. 1e, Extended Data Fig. 3b). At the position of contact with helix α2 of Tom7, hydrogen bonds among β-strands 4, 5 and 6 of Tom40 are partly broken (Fig. 1e, Extended Data Fig. 3a). The contacts of Tom5 and Tom6 with the Tom40 β-barrel are described below.

Dimer–trimer conversion

A comparison of the cryo-EM structure of the purified dimeric TOM complex with the trimer model derived from site-specific photo-crosslink mapping in intact mitochondria[4] (Extended Data Figs. 1a, 3c) showed that the relative positions of Tom5 and Tom6 to Tom40 are similar between the trimer and the dimer (Extended Data Fig. 4a). Conversely, the orientation of both Tom22 molecules and perhaps the positions of the two Tom7 molecules partially differ between the dimer and trimer (Extended Data Fig. 4a). Examination of the crosslinked residues that do not fit to the cryo-EM structure—residues 90, 309, 335 and 350 of Tom40 and residues 112 and 114 of Tom22 (Supplementary
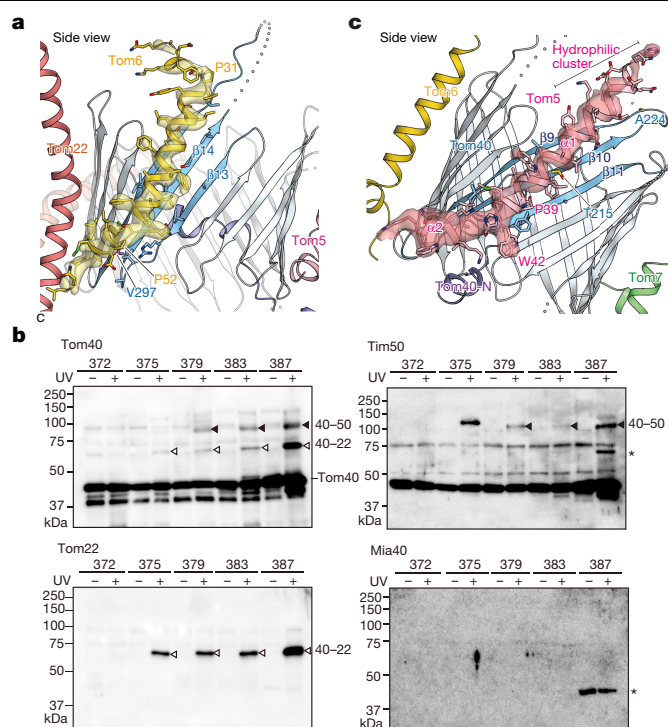

Fig. 2 | Tom5, Tom6 and the C-terminal segment of Tom40. a, Association of Tom6 (yellow, the EM density is superimposed) with the outer wall of the Tom40 β-barrel. **b**, Crosslinked products of Tom40 containing BPA at the indicated positions in the C-terminal segment were purified via His-tagged Tom40 and detected using the indicated antibodies. Crosslinked products between Tom40 and Tim50 (40–50) or Tom22 (40–22) are indicated. Blots are representative of two independent experiments. Asterisks, non-specific bands. **c**, Association of Tom5 (red, the EM density is superimposed) with the outer wall of the Tom40 β-barrel.

Table 1, Extended Data Fig. 4b, c)—suggests a possible geometrical rearrangement of the TOM subunits, including rotation of the Tom22 transmembrane helix and shift of Tom7 from the current position on dimer–trimer conversion (Extended Data Fig. 4d, e). Kinks in the membrane-embedded helices of Tom22 and Tom7 may enable twisting around the axis of the helix, potentially helping to transmit changes in positioning of the cytosolic and IMS domains of Tom22 with respect to other TOM subunits. The transmembrane helix of Tom6 also interacts with the outer wall of the Tom40 β-barrel through hydrophobic interactions with strands β13–β15 (Fig. 2a, Extended Data Fig. 3b). The initial N-terminal segment (residues 1–24) is disordered, with residues 25–31 oriented towards the neighbouring Tom40 molecule (Fig. 1b). This, together with previous crosslinking results[4,5], suggests that the transmembrane segment (residues 32–49) locks onto the β-barrel and the kinked N-terminal helix may bridge the two Tom40 molecules, providing a structural insight into how Tom6 prevents dissociation of Tom22 from the TOM complex.

The distribution of the conserved residues on the Tom40 β-barrel outer wall (Supplementary Fig. 1, Extended Data Fig. 5) shows that some key residues are distributed differently in each docking interface, suggesting specific docking interfaces for different α-helical TOM subunits. Indeed, conserved residues of the outer wall of the Tom40 β-barrel are enriched in the interface regions for Tom22 and Tom7 (Extended Data Fig. 5, Supplementary Table 2), which is consistent with the proposed ancestral TOM complex consisting of Tom40, Tom22 and Tom7[19,20]. Eight residues at conserved positions on the β-barrel surface of Tom40 were found to be in proximity to ten residues at conserved positions on the Tom22 transmembrane helices (Extended Data Fig. 5a). Two conserved residues on the Tom40 β-barrel outer wall were found
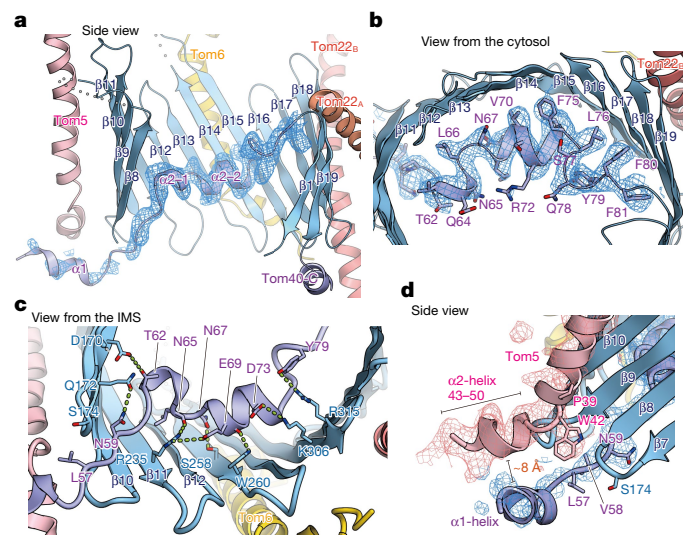
Fig. 3 | N extension of Tom40. a, Association of the α2-helix of the Tom40 N-terminal segment (dark blue, the EM density is superimposed) with the pore interior of the Tom40 β-barrel. **b**, **c**, Close-up views of the interactions between the α2-helix of the Tom40 N-terminal segment (dark blue, the EM density is superimposed) with the pore interior of the Tom40 β-barrel. **d**, Close-up view of the interactions between the α1-helix of the Tom40 N-terminal segment (dark blue, the EM density is superimposed) and the IMS region of Tom5.

to be close to two conserved residues of Tom7. In particular, G129 of Tom40, which is also conserved in another Tom7-binding protein Mdm10[25,26], may minimize possible steric hindrance in binding of the bulky side chain of conserved I33 of Tom7 to the groove of Tom40 (Extended Data Fig. 5b); W32, I33 and V36 of Tom7 are inserted into the groove formed mainly by G129, G139 and A118 of Tom40. Three residues at conserved positions of Tom40 were found to be in proximity to three residues at conserved positions of Tom6, which may be sufficient to fix the position of the transmembrane helix of Tom6 (Extended Data Fig. 5c). There was no conserved proximity pair between the Tom40 β-barrel and the Tom5 transmembrane segment (Extended Data Fig. 5d), yet the IMS segment of Tom5 interacts with the N-terminal segment of Tom40, as described below.

Exit site for the presequence pathway

Functional studies suggested that Tom7[27] and the IMS regions of Tom22[28–30] and Tom40[30,31] are involved in forming a *trans* presequence-binding site on the IMS side of the outer membrane. The proximity of the hydrophilic loop between the Tom7 helices α2 and α3, the C-terminal acidic and disordered IMS domain of Tom22 and the hydrophilic and disordered C-terminal segment and loop connecting β-strands β1 and β2 of Tom40 (Extended Data Fig. 6a, b) provides structural insight into this mechanism. In addition to the observations that the presequence of a TOM-arrested preprotein is crosslinked to Tim50[32,33] and Tim50 is in the direct vicinity of the C-terminal IMS domain of Tom22[34,35] in organello, proximity relationships of the IMS domain of Tom22, the C-terminal IMS-facing segment of Tom40 and the IMS-exposed domain of Tim50 were shown by in vivo crosslinking using photoreactive *p*-benzoylphenylalanine (BPA) (Fig. 2b, Extended Data Fig. 6c; Mia40 (also known as Tim40) was not crosslinked to the Tom22 or Tom40 C-segment, but to the Tom40 N-terminal segment, as described below). Deletion of the C-terminal segment of Tom40 impaired the accumulation of the presequence-containing Oxa1 precursor at the TOM complex *trans* site (Extended Data Fig. 6d–f), similar to the reported roles of the Tom22 IMS and Tom7 in formation of the *trans* site[27,36]. The biogenesis of the presequence-lacking precursor

of Tim9 was not inhibited by the C-terminal truncation of Tom40 (Extended Data Fig. 6g) (as described below, the import of Tim9 did not involve Tom22 or Tom7). We conclude that presequences are guided to the *trans* site composed of the IMS-facing regions of Tom40, Tom22 and Tom7 and leave the Tom40 channel in the middle of the dimeric TOM structure to be transferred from the IMS domains of Tom40 and Tom22 to Tim50 of the TIM23 complex (Extended Data Fig. 6h).

Tom5 and the N extension of Tom40

Tom5 forms a transmembrane α-helix located in the distal position of the TOM core dimer, with a kink at P39–W42 (Fig. 2c). The N-terminal hydrophilic part of the helix is oriented towards the cytosol. The central part of the Tom5 helix is hydrophobic and binds to β-strands 9–11 of Tom40. A long N-terminal segment of Tom40 (residues 1–82, termed N extension) preceding β-strand β1 passes through the β-barrel pore to the IMS side; the α1-helix (residues 48–53 of Tom40) is situated in the IMS, and the α2-helix (residues 63–74 with a short helix break at residues 66–67) is located inside the β-barrel pore (Fig. 3a–c). The α1-helix interacts with the IMS part of the Tom5 helix (Fig. 3a), whereas the α2-helix interacts with the concave inner wall of the Tom40 β-barrel (β-strands 11–17) mainly through hydrophilic residues (Fig. 3b, c).

Residues up to position 59 of the N extension are located in the proximity of the IMS part of Tom5 (Fig. 3d). We screened the growth of N-terminal and C-terminal truncation mutants of Tom40 and found that a truncation including residue 59 was critical for respiratory growth (Fig. 4a). Residue 59 is located at the beginning of the first conserved region of Tom40 (Supplementary Fig. 1). Under fermenting growth conditions, a double mutant with the N-terminal deletion Tom40(Δ59) and a deletion of *TOM5* showed a synthetic growth defect (Fig. 4b), supporting the view that Tom5 and the N extension of Tom40 are functionally related.

Exit site for proteins lacking presequences

Site-specific crosslinking revealed a close contact of small TIM chaperones to the IMS-exposed portion of the Tom40 N extension[4]. These chaperones bind the precursors of inner-membrane carrier proteins and outer-membrane β-barrel proteins upon their translocation through Tom40[1–4]. Deletion mutagenesis of the N extension of Tom40 demonstrated that removal of residues 1–57 inhibited the import of carrier precursors and β-barrel precursors, but not of presequence-containing precursors (which were inhibited by a larger truncation including residue 62)[4]. As the N extension leaves the Tom40 channel on the opposite site of the Tom22–Tom7–Tom40 *trans* site for presequence-containing precursors (Fig. 1a, b), the structure of the TOM complex reveals the existence of two different IMS exit sites of Tom40: a site for the presequence pathway located in the middle of the dimeric TOM structure and a peripheral site for the carrier and β-barrel precursors lacking a presequence (Extended Data Fig. 6h).

The fourth essential protein import pathway of mitochondria transports cysteine-rich precursors through the TOM complex to the mitochondrial IMS import and assembly (MIA) system[37–40]. The core component Mia40 was crosslinked to the disordered Tom40 N extension via BPA introduced at residues 34 and 44 of the extension (Fig. 4c), suggesting that the N extension recruits Mia40 to the IMS outlet of the Tom40 channel (Tom22 and Tim50 were crosslinked not to the N extension, but to the C-segment of Tom40; Fig. 2b). The import of MIA substrates such as Tim9 was highly dependent on the presence of Tom5, but not on other small TOM proteins or TOM receptors[38,41] (Extended Data Fig. 7a–e); in Tom40(Δ59) mitochondria, the steady-state level of Tom5 decreased at elevated temperature (37 °C) (Extended Data Fig. 7f); the isolated mitochondria were competent in inserting the Tom5 precursor into the outer membrane (Extended Data Fig. 7g), indicating that the N extension of Tom40 stabilizes the assembly of Tom5
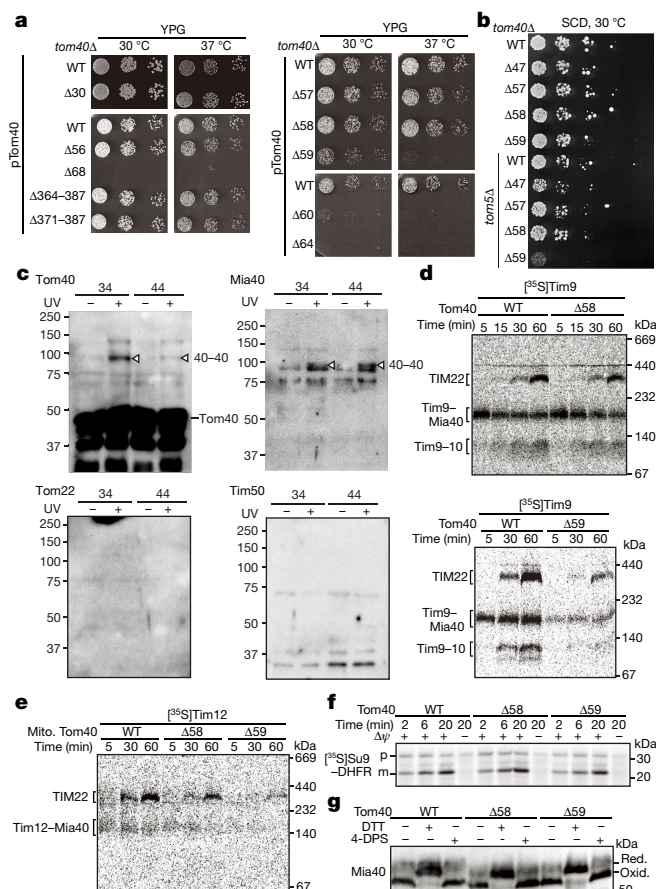
Fig. 4 | The N extension of Tom40 recruits Mia40 and promotes import of MIA substrates. a, Growth analysis of yeast strains expressing Tom40 variants with the indicated N- or C-terminal truncations on non-fermentable medium. Data are representative of three independent experiments. WT, wild-type. **b**, Growth analysis of wild-type and *tom5Δ* strains expressing the indicated Tom40 N-terminal truncations on fermentable medium. Data are representative of two independent experiments. **c**, Crosslinked products of Tom40 containing BPA at the indicated positions were purified via His-tagged Tom40 and detected by the indicated antibodies. Crosslinked products between Tom40 and Mia40 (40–40) are indicated. Blots are representative of three (top left) or two (other blots) independent experiments. **d**, **e**, Import of radiolabelled Tim9 and Tim12 into isolated wild-type, Tom40(Δ58) and Tom40(Δ59) mitochondria, followed by analysis via native gel electrophoresis and autoradiography. Data are representative of three (**d**) or two (**e**) independent experiments. TIM22, TIM22 complex; Tim9–Mia40 and Tim12–Mia40, mixed disulfide intermediates of Tim precursors with Mia40. **f**, Import of radiolabelled pSu9–DHFR into isolated mitochondria, followed by treatment with proteinase K and SDS–PAGE analysis. Data are representative of two independent experiments. Δψ, membrane potential; p, precursor form; m, mature form. **g**, Wild-type, Tom40(Δ58) and Tom40(Δ59) mitochondria were treated with 4,4′-dipyridyl disulfide (4-DPS) or dithiothreitol (DTT) and the redox state of Mia40 was analysed by non-reducing SDS–PAGE and western blotting. Data are representative of two independent experiments. Red., reduced form; oxid., oxidized form.
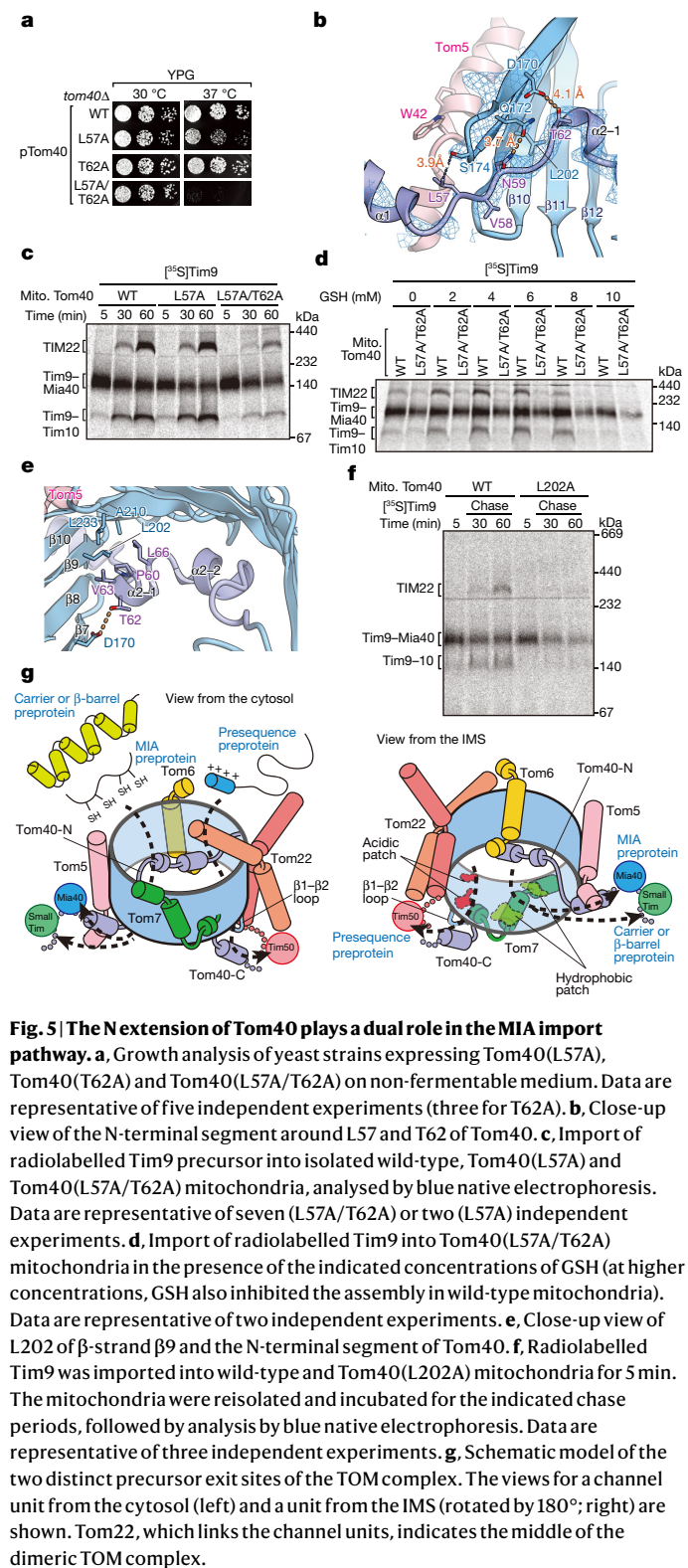
into the TOM complex. To analyse whether the N extension itself has a role in the MIA import pathway, we isolated mitochondria from cells grown at 30 °C that contained wild-type levels of Tom5 (Extended Data Fig. 7f). Under these conditions, the TOM complex analysed by native gel electrophoresis became smaller owing to the truncation of Tom40, but formed a stable complex; only a small fraction was destabilized in Tom40(Δ59) mitochondria (Extended Data Fig. 7h). The biogenesis of MIA substrates (Tim9 and Tim12) can be dissected in an early targeting step to the Mia40-bound intermediate and a late folding/assembly step

into the oxidized Tim9–Tim10 and TIM22 complexes[39,42]. Tom40(Δ59) mitochondria were impaired in the early targeting to Mia40, and therefore the late folding/assembly step was diminished (Fig. 4d, e). The presequence import pathway, analysed with the Atp2 precursor and model preproteins Su9–mouse dihydrofolate reductase (Su9–DHFR) and b₂(167)ΔDHFR, was not affected in these Tom40 mutants (Fig. 4f, Extended Data Fig. 7i). The redox state and native electrophoretic mobility of Mia40 and the intactness of the outer membrane (Fig. 4g, Extended Data Fig. 7h, j) were not altered in the Tom40 truncation mutants, excluding the possibility that the import of MIA substrates was indirectly affected by an altered Mia40 activity or the loss of IMS components.

The results so far suggest that the N extension of Tom40 interacts with Tom5. Tom5 and the IMS-exposed portion of the N extension including residue 59 are required for the efficient targeting of precursors to Mia40, indicating that, like carrier and β-barrel precursors, MIA substrates leave the Tom40 channel near the N extension–Tom5 (Extended Data Fig. 6h).

Point mutations in the conserved Tom40 residues L57 and T62 showed a synthetic growth defect (Fig. 5a). T62 of the N extension interacts with D170 in strand β7 of the β-barrel wall, whereas L57 is in the vicinity of S174 in the loop connecting the β7 and β8 strands (Fig. 5b); Tom5 and Mia40 interacting regions are retained in these point mutants. In Tom40(L57A/T62A) double-mutant mitochondria, the early targeting of Tim9 precursor to the Mia40-bound intermediate was possible, but the late biogenesis step towards formation of oxidized Tim9–Tim10 and TIM22 complexes was impaired (Fig. 5c). The presequence and carrier import pathways (Su9–DHFR and ADP–ATP carrier (AAC), respectively) were unaffected or only mildly affected in Tom40(L57A/T62A) mitochondria (Extended Data Fig. 7k). Addition of reduced glutathione (GSH) promotes the formation of oxidized MIA pathway substrates, probably by preventing the formation of non-productive long-lived Mia40-substrate intermediates[43]. GSH stimulated Tim9 assembly in wild-type mitochondria, but not in Tom40 (L57A/T62A) mitochondria (Fig. 5d). Tom5 levels, TOM native electrophoretic mobility and Mia40 redox state were similar to the wild type in Tom40(L57A/T62A) mitochondria (Extended Data Figs. 7l, 8a, b). We conclude that these conserved Tom40 residues are involved in promoting late steps of the MIA pathway, including oxidative folding and subsequent assembly into the final complexes. This is consistent with the report that deletion of the conserved NPGT sequence in *Neurospora crassa* Tom40 (corresponding to yeast residues 59–62; Supplementary Fig. 1) caused severe growth defects[44].

Replacement of the conserved residue L202 in the Tom40 β9-strand by alanine (Supplementary Fig. 1) caused respiratory growth defects at elevated temperature (Extended Data Fig. 8c). L202 appears to be responsible for the positioning of helix α2 of the N extension by forming a hydrophobic linkage to type-conserved V63 and L66 in the N extension together with type-conserved A210 and L233 in the inner wall of the Tom40 β-barrel (Fig. 5e, Supplementary Fig. 1). The precursor of Tim9 was targeted to Mia40 in Tom40(L202A) mitochondria, but the subsequent chase into the oxidized form, which involves the formation of intramolecular disulfide bonds[42,45], was impaired (Fig. 5f), similar to the effect of iodoacetamide addition to prevent formation of further disulfides in the precursor (Extended Data Fig. 8d). Tom40(L202A) mitochondria accumulated the Tim9(C55S) variant precursor[42] as the Mia40 mixed disulfide intermediate with an efficiency close to that of wild-type mitochondria (Extended Data Fig. 8e), offering further evidence that targeting to Mia40 was possible in Tom40(L202A) mitochondria. The Tim9 precursor was lost from Tom40(L202A) mitochondria when the chase to the oxidized forms was attempted (Fig. 5f), but not when the oxidation was blocked by iodoacetamide; that is, when the precursor remained bound to Mia40 (Extended Data Fig. 8d). The Mia40 redox state, TOM native electrophoretic mobility, intactness of the outer membrane, presequence and carrier import pathways

Fig. 5 | The N extension of Tom40 plays a dual role in the MIA import pathway. a, Growth analysis of yeast strains expressing Tom40(L57A), Tom40(T62A) and Tom40(L57A/T62A) on non-fermentable medium. Data are representative of five independent experiments (three for T62A). **b**, Close-up view of the N-terminal segment around L57 and T62 of Tom40. **c**, Import of radiolabelled Tim9 precursor into isolated wild-type, Tom40(L57A) and Tom40(L57A/T62A) mitochondria, analysed by blue native electrophoresis. Data are representative of seven (L57A/T62A) or two (L57A) independent experiments. **d**, Import of radiolabelled Tim9 into Tom40(L57A/T62A) mitochondria in the presence of the indicated concentrations of GSH (at higher concentrations, GSH also inhibited the assembly in wild-type mitochondria). Data are representative of two independent experiments. **e**, Close-up view of L202 of β-strand β9 and the N-terminal segment of Tom40. **f**, Radiolabelled Tim9 was imported into wild-type and Tom40(L202A) mitochondria for 5 min. The mitochondria were reisolated and incubated for the indicated chase periods, followed by analysis by blue native electrophoresis. Data are representative of three independent experiments. **g**, Schematic model of the two distinct precursor exit sites of the TOM complex. The views for a channel unit from the cytosol (left) and a unit from the IMS (rotated by 180°; right) are shown. Tom22, which links the channel units, indicates the middle of the dimeric TOM complex.

were not affected in Tom40(L202A) mitochondria (Extended Data Fig. 8b, g, h).

We conclude that the N extension of Tom40 plays a dual role in the MIA pathway. First, the IMS-exposed portion of the extension (up to residue 59) interacts with Mia40 and Tom5 and is required for the early import step—that is, translocation of precursors to Mia40 and formation of a Mia40-precursor mixed intermediate. Second, Tom40 residues involved in the positioning of the N extension inside the β-barrel

(including residues 57, 62 and 202) are required for late biogenesis steps that involve the complete import of precursors into the IMS and the formation of intramolecular disulfide bonds. Mutants in which this late biogenesis step is disturbed exhibited a loss of precursor from mitochondria, indicating that the full translocation of the precursor through Tom40 occurs only at this late stage.

Conclusions

Four protein import pathways into mitochondria are essential for cell viability. In each of these pathways, the precursor proteins are translocated through the TOM complex. The cryo-EM structure of the core TOM complex reveals an α/β-membrane-integrated translocator. Given that the core machinery is conserved in all eukaryotes[19,20], the structure of the TOM complex from yeast provides a fundamental model for the function of this exquisite nanomachine. Conserved proline residues provide kinks in the α-helical transmembrane segments that cope with embracing the rounded outer face of the Tom40 β-barrel and provide intricate structural features such as the Tom7 crook into the presequence-binding domain and a potential Tom22 rotational manoeuvre for opening of the putative lateral gate in Tom40.

The β-barrel structure of Tom40 discloses surfaces that are proposed to guide protein substrates through the Tom40 channel[4] (Extended Data Fig. 9). Site-specific crosslinking indicated that presequences and hydrophobic precursors interact with different residues of the channel interior[4]. The cryo-EM structure demonstrates the inferred alignment[4] of acidic patches and hydrophobic patches, respectively, and thus outlines different translocation paths for presequence-containing precursors and hydrophobic precursors. The N extension of Tom40 passes through the β-barrel into the IMS. Full activity of the MIA import pathway depends on proper positioning of the N extension inside the barrel lumen.

The TOM structure reveals two preprotein exit sites towards the IMS (Fig. 5g). Presequence-containing preproteins that constitute around 60% of mitochondrial proteins leave the Tom40 pore at the *trans* presequence-binding site, which is formed by Tom22–Tom7–Tom40 near the middle of the Tom40 dimer, and are then transferred to Tim50 of the TIM23 complex. Presequence-lacking preproteins, which include three different classes (MIA substrates, β-barrel and carrier precursors), leave the Tom40 channel in the proximity of Tom5 and the N extension of Tom40 at the periphery of the Tom40 dimer. The IMS-exposed portion of the N extension of Tom40 recruits small TIM chaperones and Mia40 close to the exit site to ensure an efficient transfer of precursor proteins. The TOM complex thus functions as a hub for the intramitochondrial sorting of precursor proteins.

Online content

Any methods, additional references, Nature Research reporting summaries, source data, extended data, supplementary information, acknowledgements, peer review information; details of author contributions and competing interests; and statements of data and code availability are available at https://doi.org/10.1038/s41586-019-1680-7.

1. Endo, T. & Yamano, K. Multiple pathways for mitochondrial protein traffic. *Biol. Chem.* **390**, 723–730 (2009).
2. Neupert, W. A perspective on transport of proteins into mitochondria: a myriad of open questions. *J. Mol. Biol.* **427**, 1135–1158 (2015).
3. Pfanner, N., Warscheid, B. & Wiedemann, N. Mitochondrial proteins: from biogenesis to functional networks. *Nat. Rev. Mol. Cell Biol.* **20**, 267–284 (2019).
4. Shiota, T. et al. Molecular architecture of the active mitochondrial protein gate. *Science* **349**, 1544–1548 (2015).
5. Sakaue, H. et al. Porin associates with Tom22 to regulate the mitochondrial protein gate assembly. *Mol. Cell* **73**, 1044–1055 (2019).
6. Künkele, K.-P. et al. The preprotein translocation channel of the outer membrane of mitochondria. *Cell* **93**, 1009–1019 (1998).
7. Ahting, U. et al. The TOM core complex: the general protein import pore of the outer membrane of mitochondria. *J. Cell Biol.* **147**, 959–968 (1999).

8. Model, K., Meisinger, C. & Kühlbrandt, W. Cryo-electron microscopy structure of a yeast mitochondrial preprotein translocase. *J. Mol. Biol.* **383**, 1049–1057 (2008).
9. Bausewein, T. et al. Cryo-EM structure of the TOM core complex from *Neurospora crassa*. *Cell* **170**, 693–700 (2017).
10. Van den Berg, B. et al. X-ray structure of a protein-conducting channel. *Nature* **427**, 36–44 (2004).
11. Voorhees, R. M., Fernández, I. S., Scheres, S. H. W. & Hegde, R. S. Structure of the mammalian ribosome–Sec61 complex to 3.4 Å resolution. *Cell* **157**, 1632–1643 (2014).
12. Gogala, M. et al. Structures of the Sec61 complex engaged in nascent peptide translocation or membrane insertion. *Nature* **506**, 107–110 (2014).
13. Itskanov, S. & Park, E. Structure of the posttranslational Sec protein–translocation channel complex from yeast. *Science* **363**, 84–87 (2019).
14. Wu, X., Cabanos, C. & Rapoport, T. A. Structure of the post-translational protein translocation machinery of the ER membrane. *Nature* **566**, 136–139 (2019).
15. Baud, C. et al. Translocation path of a substrate protein through its Omp85 transporter. *Nat. Commun.* **5**, 5271 (2014).
16. Lundquist, K., Bakelar, J., Noinaj, N. & Gumbart, J. C. C-terminal kink formation is required for lateral gating in BamA. *Proc. Natl Acad. Sci. USA* **115**, E7942–E7949 (2018).
17. Bamert, R. S. et al. Structural basis for substrate selection by the translocation and assembly module of the β-barrel assembly machinery. *Mol. Microbiol.* **106**, 142–156 (2017).
18. Model, K. et al. Protein translocase of the outer mitochondrial membrane: role of import receptors in the structural organization of the TOM complex. *J. Mol. Biol.* **316**, 657–666 (2002).
19. Dolezal, P., Likic, V., Tachezy, J. & Lithgow, T. Evolution of the molecular machines for protein import into mitochondria. *Science* **313**, 314–318 (2006).
20. Fukasawa, Y., Oda, T., Tomii, K. & Imai, K. Origin and evolutionary alteration of the mitochondrial import system in eukaryotic lineages. *Mol. Biol. Evol.* **34**, 1574–1586 (2017).
21. Maćasev, D. et al. Tom22', an 8-kDa trans-site receptor in plants and protozoans, is a conserved feature of the TOM complex that appeared early in the evolution of eukaryotes. *Mol. Biol. Evol.* **21**, 1557–1564 (2004).
22. Senes, A., Gerstein, M. & Engelman, D. M. Statistical analysis of amino acid patterns in transmembrane helices: the GxxxG motif occurs frequently and in association with β-branched residues at neighboring positions. *J. Mol. Biol.* **296**, 921–936 (2000).
23. Harner, M., Neupert, W. & Deponte, M. Lateral release of proteins from the TOM complex into the outer membrane of mitochondria. *EMBO J.* **30**, 3232–3241 (2011).
24. Höhr, A. I. C. et al. Membrane protein insertion through a mitochondrial β-barrel gate. *Science* **359**, eaah6834 (2018).
25. Yamano, K., Tanaka-Yamano, S. & Endo, T. Tom7 regulates Mdm10-mediated assembly of the mitochondrial import channel protein Tom40. *J. Biol. Chem.* **285**, 41222–41231 (2010).
26. Ellenrieder, L. et al. Separating mitochondrial protein assembly and endoplasmic reticulum tethering by selective coupling of Mdm10. *Nat. Commun.* **7**, 13021 (2016).
27. Esaki, M. et al. Mitochondrial protein import. Requirement of presequence elements and TOM components for precursor binding to the TOM complex. *J. Biol. Chem.* **279**, 45701–45707 (2004).
28. Court, D. A. et al. Role of the intermembrane-space domain of the preprotein receptor Tom22 in protein import into mitochondria. *Mol. Cell. Biol.* **16**, 4035–4042 (1996).
29. Moczko, M. et al. The intermembrane space domain of mitochondrial Tom22 functions as a *trans* binding site for preproteins with N-terminal targeting sequences. *Mol. Cell. Biol.* **17**, 6574–6584 (1997).
30. Kanamori, T. et al. Uncoupling of transfer of the presequence and unfolding of the mature domain in precursor translocation across the mitochondrial outer membrane. *Proc. Natl Acad. Sci. USA* **96**, 3634–3639 (1999).
31. Rapaport, D., Neupert, W. & Lill, R. Mitochondrial protein import. Tom40 plays a major role in targeting and translocation of preproteins by forming a specific binding site for the presequence. *J. Biol. Chem.* **272**, 18725–18731 (1997).
32. Yamamoto, H. et al. Tim50 is a subunit of the TIM23 complex that links protein translocation across the outer and inner mitochondrial membranes. *Cell* **111**, 519–528 (2002).
33. Mokranjac, D. et al. Tim50, a novel component of the TIM23 preprotein translocase of mitochondria. *EMBO J.* **22**, 816–825 (2003).
34. Shiota, T., Mabuchi, H., Tanaka-Yamano, S., Yamano, K. & Endo, T. In vivo protein-interaction mapping of a mitochondrial translocator protein Tom22 at work. *Proc. Natl Acad. Sci. USA* **108**, 15179–15183 (2011).
35. Tamura, Y. et al. Tim23–Tim50 pair coordinates functions of translocators and motor proteins in mitochondrial protein import. *J. Cell Biol.* **184**, 129–141 (2009).
36. Chacinska, A. et al. Mitochondrial presequence translocase: switching between TOM tethering and motor recruitment involves Tim21 and Tim17. *Cell* **120**, 817–829 (2005).
37. Naoé, M. et al. Identification of Tim40 that mediates protein sorting to the mitochondrial intermembrane space. *J. Biol. Chem.* **279**, 47815–47821 (2004).
38. Gornicka, A. et al. A discrete pathway for the transfer of intermembrane space proteins across the outer membrane of mitochondria. *Mol. Biol. Cell* **25**, 3999–4009 (2014).
39. Chacinska, A. et al. Essential role of Mia40 in import and assembly of mitochondrial intermembrane space proteins. *EMBO J.* **23**, 3735–3746 (2004).
40. Mesecke, N. et al. A disulfide relay system in the intermembrane space of mitochondria that mediates protein import. *Cell* **121**, 1059–1069 (2005).
41. Kurz, M. Martin, H. Rassow, J., Pfanner, N. & Ryan, M. T. Biogenesis of Tim proteins of the mitochondrial carrier pathway: differential targeting mechanisms and crossing over with the main import pathway. *Mol. Biol. Cell* **10**, 2461–2474 (1999).
42. Stojanovski, D. et al. Mitochondrial protein import: precursor oxidation in a ternary complex with disulfide carrier and sulfhydryl oxidase. *J. Cell Biol.* **183**, 195–202 (2008).
43. Bien, M. et al. Mitochondrial disulfide bond formation is driven by intersubunit electron transfer in Erv1 and proofread by glutathione. *Mol. Cell* **37**, 516–528 (2010).
44. Rapaport, D. et al. Structural requirements of Tom40 for assembly into preexisting TOM complexes of mitochondria. *Mol. Biol. Cell* **12**, 1189–1198 (2001).
45. Habich, M. et al. Vectorial import via a metastable disulfide-linked complex allows for a quality control step and import by the mitochondrial disulfide relay. *Cell Rep.* **26**, 759–774 (2019).
46. Becker, T. et al. Role of phosphatidylethanolamine in the biogenesis of mitochondrial outer membrane proteins. *J. Biol. Chem.* **288**, 16451–16459 (2013).

Article

Methods

No statistical methods were used to predetermine sample size. The experiments were not randomized, and investigations were not blinded to allocation during experiments and outcome assessment.

Protein expression and purification

The TOM complex was purified from the *S. cerevisiae* strain expressing Tom22 with the C-terminally attached His$_{10}$ tag from the chromosome (the *Tom22-His10-pep4Δ* strain). After cultivation in 24 l YPD medium for 24 h at 30 °C, cells were collected and resuspended in 10–20 ml of breaking buffer (0.6 M sorbitol, 10 mM Tris-HCl, pH 7.4, 1 mM EDTA). The cells were frozen by dropwise addition to liquid nitrogen in a 1000 ml stainless beaker to form small particles, which were subsequently grounded by Multi-Beads Shocker (Yasui Kikai). The resultant frozen cell powder was slowly thawed at room temperature and centrifuged (1,500g, 20 min, 4 °C) to remove debris. Mitochondria were isolated by centrifugation (13,000g, 20 min, 4 °C) and washed by SEM buffer (250 mM sucrose, 10 mM MOPS, pH 7.2, 1 mM EDTA). After lysis of mitochondria with solubilization buffer (50 mM Hepes-KOH, pH 7.4, 150 mM NaCl, 5% glycerol and 1.1% digitonin (Merck)) for 16 h at 4 °C, insoluble materials were removed by centrifugation (23,000g, 30 min, 4 °C). The supernatant was mixed with 2 ml of TALON metal affinity resin (Clontech) and incubated for 30 min. The TOM complex was eluted by step gradient of 10–160 mM imidazole in TALON buffer (20 mM Hepes-KOH, pH 7.4, 150 mM NaCl, 0.1% GDN (Anatrace)). The eluted fraction was subjected to gel filtration with a Superose 6 Increase 10/300 GL column (GE Healthcare) equilibrated with gel-filtration buffer (20 mM Hepes-KOH, pH 7.4, 150 mM NaCl, 0.01% GDN). The purified TOM complex was concentrated to 5-10 mg ml^{-1} with an Amicon Ultra-0.5 filter (Merck Millipore, 100 kDa MW cut-off).

Cryo-EM grid preparation

The concentrated TOM complex was loaded onto a glow-discharged grid (Quantifoil R1.2/1.3, Cu/Rh, 200 mesh), blotted by Vitrobot Mark IV (FEI) at 6 °C, and plunge-frozen in liquid ethane.

Cryo-EM data acquisition and processing

Grids were screened for ice quality and cryo-EM data were acquired on a Titan Krios transmission EM (Thermo Fisher Scientific) at 300 kV under low-dose conditions (49 frames at 50 e^- Å^{-2}). A total of 2,057 micrographs were collected on a Falcon III direct electron detector (Thermo Fisher Scientific). The movie frames were aligned using MotionCor2[47]. CTF parameters were estimated by CTFFIND 4[48]. Then, 1,866 micrographs were submitted to auto-picking. Subsequently, 699,268 particles were extracted and 2D classified by RELION-3.0[49]. For building an initial model, an additional two rounds of 2D classification were performed. Selected 573,344 particles from the first 2D classification were submitted to 3D classification, with the initial model as 3D reference. Two rounds of 3D classification were performed, the first one with no symmetry and the subsequent second one with C2 symmetry imposed. Finally, 124,653 particles were selected for several cycles of 3D auto-refinement followed by CTF refinement and Bayesian polishing (Extended Data Table. 1). The overall gold-standard resolution was 3.81 Å, with the local resolution in the N-terminal helix of the Tom40 channel extending to 3.66 Å.

Model building and refinement

The atomic models of all five different subunits of the TOM complex were built de novo into the EM density map in COOT[50]. As guide structures, we used a homology model of *S. cerevisiae* (*Sc*) Tom40 based on the *N. crassa* (*Nc*) Tom40 model (PDB: 5O8O) and the cryo-EM structure of *Nc*TOM complex (EMDB: 3761). The atomic model of the *Sc*TOM complex was refined using PHENIX[51]. Molecular graphics were illustrated with UCSF Chimera[52], Molecular Operating Environment (MOE) software (2016.08; Chemical Computing Group) and CueMol 2.0 (http://www.cuemol.org).

Yeast strains, plasmids and primers

The *S. cerevisiae* strains used in this study are listed in Supplementary Table 3[53]. For the preparation of the yeast TOM complex, the DNA fragments for Tom22−His10[34] and the *kanMX4* marker were combined by PCR using the primers Tom22His10-KanMX-f and Tom22His10-KanMX-r (Supplementary Table 4) and integrated into the *TOM22* locus of the D273-10B strain, then G418+ transformants were selected to yield the *Tom22-His10* strain. The DNA fragment for *YAP1* was amplified by PCR using primers of PEP4-YAP1-f and PEP4-YAP1-r (Supplementary Table 4), and was integrated into the *PEP4* locus in the *Tom22-His10* strain, then cycloheximide resistant transformants were selected to yield the *Tom22-His10-pep4Δ* strain.

The strains *tom5Δ*, *tom6Δ*, *tom7Δ*, *tom20Δ*, *tom22Δ*, *tom70Δ* and their corresponding wild-type strains YPH499 and YPH500 have been described[54,55]. Yeast strains expressing wild-type or mutant Tom40 proteins except for those in Fig. 4b were generated by transforming pFL39-*TOM40* or the related plasmids encoding Tom40 mutant versions into the yeast strain YPH499-*tom40Δ* + Yep-*TOM40* followed by selection on 5-fluoroorotic acid (5-FOA) plates (9.33 mM 5-FOA (MEL-FORD), 1.68% (w/v) yeast nitrogen base without amino acids (Difco, BD), 5% (w/v) glucose and 0.19% (w/v) CSM-URA (MP Biomedicals), 0.013% (w/v) uracil (Sigma)). Yeast cells were grown in YPD (1% (w/v) yeast extract, 2% (w/v) bacto peptone, 2% (w/v) glucose), YPS (1% (w/v) yeast extract, 2% (w/v) bacto peptone, 2% (w/v) sucrose) or YPG (1% (w/v) yeast extract, 2% (w/v) bacto peptone, 3% (w/v) glycerol, pH 5.0) at 24–30 °C. For growth analysis, yeast cells grown in YPD until OD$_{600}$ 1.0 were diluted to OD$_{600}$ 0.01 in sterilized water[56]. The cells were plated at fivefold serial dilution on YPD or YPG plates.

To construct the strain W303-1A-*tom40Δtom5Δ* + pRS316-*TOM40*, the DNA fragment for the *hygMX* marker was amplified by PCR using the primers tom5-del-fw and tom51-del-rv from the pBS-hygMX plasmid. The amplified DNA fragment was integrated into the 3′-half region of the *TOM5* gene, and hygromycin B-resistant transformants were selected. Yeast strains used in Fig. 4b were further generated by transforming pRS314-*TOM40* or the related plasmids encoding Tom40 mutants into the strains W303-1A-*tom40Δ* + pRS316-*TOM40* or W303-1A-*tom40Δtom5Δ* + pRS316-*TOM40* followed by cultivation in SCD medium (0.67% (w/v) yeast nitrogen base without amino acids (Difco, BD), 2% (w/v) glucose (Nacalai Tesque), 0.5% (w/v) casamino acid (Difco, BD), 0.002% (w/v) uracil (Fuji-film Wako)) containing 5.2 mM 5-FOA. For growth analysis, yeast cells were plated at tenfold dilution on SCD (with 5.2 mM 5-FOA) plates at 30 °C.

Cloning

The DNA constructs for the N-terminally truncated Tom40 mutants except for those used for Fig. 4b were made by two-step PCR based on pFL39-*TOM40*. The first round of PCR was performed using primer sets Tom40up/Tom40R and Tom40Δ2-x/Tom40down (x represents the C-terminal amino-acid position of the truncated region), respectively (Supplementary Table 4). The resulting PCR products were mixed in equimolar amounts as template and amplified using the primer set Tom40up/Tom40down to generate the final PCR product, which was subsequently digested with BamHI and HincII to replace the corresponding fragment of pFL39-*TOM40*. The DNA constructs for the C-terminally truncated Tom40 mutants were generated using the same strategy. The first round of PCR was performed using primer sets Tom40Cup/Tom40Δy-387 and Tom40CF/Tom40Cdown (y represents the N-terminal amino-acid position of the truncated region), respectively. The resulting PCR products were mixed in equimolar amounts as template and amplified using the primer set Tom40Cup/Tom40Cdown to generate the final PCR product, which was subsequently digested with HincII and HindIII to replace the corresponding

fragment of pFL39-*TOM40*. All point mutations were introduced by the QuikChange Site-Directed Mutagenesis Kit (Agilent Technologies) using the corresponding primer pairs (Supplementary Table 4) according to the manufacturer's instructions based on pFL39-*TOM40*. The plasmid pFL39-Tom40-L57A/T62A was generated by introducing L57A via the primer set L57Afw/L57Arv into the plasmid pFL39-Tom40-T62A. All plasmids were sequenced. Besides the expected mutations, the plasmids encoding Tom40 truncation mutants (except pFL39-Tom40-Δ364-387) and Tom40-T62A contained an undesired mutation, which led to an E360G substitution in the translated protein. For these mutants, pFL39-Tom40-E360G, which did not lead to any growth phenotype of yeast cells compared to pFL39-*TOM40*, served as the control plasmid.

The DNA constructs for wild-type Tom40 and the N-terminally truncated Tom40 mutants used for Fig. 4b were made as follows. The pRS314 plasmid containing the *TOM40* promoter and terminator containing the BamHI/XhoI site in between them were used to integrate the DNA fragments for Tom40 or its N-terminally truncated mutants that were PCR-amplified with the primer pairs of Tom40-fw or tom40Δz-fw (z represents the N-terminal amino-acid position of the truncated region) and Tom40-rv (Supplementary Table 4) at the BamHI/XhoI site.

HS-AFM observation
HS-AFM observation was performed in the tapping mode using a laboratory-built apparatus[57]. The short cantilevers used (BL-AC10DS-A2) were purchased from Olympus; resonant frequency, ~600 KHz in water; quality factor, ~2 in water; and spring constant, ~0.1 N/m. The general procedure for HS-AFM observation of protein molecules was described previously[58]. In brief, a glass sample stage (diameter, ~2 mm; height, ~2 mm) with a thin mica disc (1 mm in diameter and 0.05 mm thick) glued to the top by epoxy was attached onto the top of the *Z*-scanner by a drop of nail polish. A freshly cleaved mica surface was prepared by removing the top layers of mica using Scotch tape. Then, a drop (~2 µl) of the solubilized TOM complex diluted with a buffer containing 20 mM Hepes-KOH (pH 7.4), 150 mM KCl and 0.01% GDN (final concentration of the TOM complex 0.25 nM) was deposited onto the mica surface. After 5 min of incubation, the sample stage was immersed in a liquid cell containing ~60 µl of the same buffer. The cantilever's free oscillation amplitude A_0 was set at 1–2 nm and the set point amplitude was set at $0.9 \times A_0$, such that the loss of cantilever's oscillation energy per tap was adjusted to be 2–3 $k_B T$ on average. The imaging rate, scan size and pixel size were a combination of 5 frames s^{-1}, 50×50 nm^2 and 50×50 or of 3.3 frames s^{-1}, 200×200 nm^2 and 120×120, respectively.

Isolation of mitochondria
Yeast cells were grown in YPG, YPS or YPD at 24–37 °C until an early logarithmic growth phase. Mitochondria were isolated by differential centrifugation[55]. Yeast cells were collected, washed in water and incubated in prewarmed DTT softening buffer (100 mM Tris-H$_2$SO$_4$, pH 9.4, 10 mM DTT) for 20 min at growth temperature. Cells were washed and incubated in zymolyase buffer (20 mM K$_2$HPO$_4$, pH 7.4, 1.2 M sorbitol) supplemented with 4 mg per g cells zymolyase (Seikagaku Biobusiness) at growth temperature for 30 min to open the cell wall. The obtained spheroplasts were washed and homogenized in cold homogenizing buffer (600 mM sorbitol, 10 mM Tris-HCl, pH 7.4, 1 mM EDTA, 0.2% (w/v) fatty-acid free bovine serum albumin, 2 mM PMSF) using a teflon glass homogenizer. Subsequently, cell debris was removed (2,700*g*, 6 min, 4 °C) and mitochondria were isolated from the supernatant (17,000*g*, 15 min, 4 °C). Mitochondria were resuspended in SEM buffer (250 mM sucrose, 1 mM EDTA, 10 mM MOPS, pH 7.2) at a protein concentration of 10 mg ml^{-1} and were shock-frozen in liquid nitrogen. Mitochondria were stored in aliquots at −80 °C until use. For western blotting, mitochondrial proteins were separated by blue native electrophoresis or SDS–PAGE. To compare the levels of various proteins in parallel, the identical batches of isolated mitochondria were loaded onto several gels in order to obtain the optimal separation range for decoration with specific antisera for each protein of interest.

Synthesis of radiolabelled precursor proteins
To generate radiolabelled mitochondrial precursor proteins, pGEM4Z plasmids or PCR-generated templates were used for in vitro translation in the presence of [^{35}S]methionine by the Flexi Rabbit Reticulocyte Lysate System (Promega) or the TNT SP6 Coupled Reticulocyte Lysate System (Promega) according to the manufacturer's instructions. To prepare Tim9 precursors for import, lysates were either treated with 10 mM DTT and used for import experiments or precipitated with two volumes of saturated (NH$_4$)$_2$SO$_4$ supplemented with 20 mM EDTA and 50 mM DTT for 30 min on ice. After centrifugation (20,000*g*, 15 min, 4 °C), the precipitated proteins were resuspended in urea denaturation buffer (8 M urea, 30 mM MOPS, pH 7.2, 20 mM DTT) and shaken at 25 °C for 15 min. After a clarifying spin (20,000*g*, 5 min, room temperature), the supernatant containing denatured Tim9 precursors was used for import experiments.

Mitochondrial protein import
The import of small Tim precursors was performed according to the previously reported method[59]. In brief, Tim9 precursors were incubated at 30 °C for the indicated periods with isolated mitochondria in import buffer lacking BSA (250 mM sucrose, 80 mM KCl, 5 mM MgCl$_2$, 10 mM KH$_2$PO$_4$, 5 mM L-methionine, 10 mM MOPS-KOH, pH 7.2) supplemented with 2–10 mM GSH when indicated. The import reaction was stopped by addition of iodoacetamide to 50 mM final concentration. To chase the precursor, mitochondria were reisolated after 5 min import and subsequently resuspended in the import buffer without BSA for the chasing period. To remove the small Tim precursors exposed on the mitochondrial surface after import, the samples were treated with 10 µg ml^{-1} proteinase K for 15 min on ice. To study the arrest of Tim9 precursors at the Mia40 stage after 5 min import, samples were treated with 50 mM (final concentration) iodoacetamide and were further incubated at 30 °C for the indicated periods. Other radiolabelled precursor proteins were incubated with isolated mitochondria in import buffer (3% (w/v) fatty-acid free BSA, 250 mM sucrose, 80 mM KCl, 5 mM MgCl$_2$, 2 mM KH$_2$PO$_4$, 5 mM L-methionine, 10 mM MOPS-KOH pH 7.2) supplemented with 4 mM ATP, 4 mM NADH, 5 mM creatine phosphate and 0.1 mg ml^{-1} creatine kinase at 20 °C or 25 °C for the indicated periods. To dissipate the membrane potential ($\Delta\psi$), 8 µM antimycin A, 1 µM valinomycin and 20 µM oligomycin were used. After import, the samples were treated with proteinase K (25–50 µg ml^{-1}) for 15 min on ice where indicated. To study the insertion of Tom5 into the outer membrane, radiolabelled Tom5 precursor was incubated in import buffer for 10 min at 25 °C. After a clarifying spin to remove aggregated precursor, isolated mitochondria were added, followed by an import incubation at 25 °C. The mitochondria were reisolated immediately after the import incubation, washed and incubated in 0.1 M sodium carbonate. After 30 min on ice, carbonate-resistant membrane sheets were pelleted (125,000*g*, 30 min, 4 °C) and analysed by SDS–PAGE[60].

Proteinase K treatment, reduction and oxidation of mitochondrial proteins
Isolated mitochondria were incubated in SEM buffer or EM buffer (1 mM EDTA, 10 mM MOPS, pH 7.2) for 15 min on ice. Subsequently, mitochondria were treated with 10–50 µg ml^{-1} proteinase K for 15 min on ice. To inhibit the proteinase K activity, mitochondria were incubated with 2 mM PMSF for 10 min on ice. To reduce or oxidize mitochondrial proteins, isolated mitochondria were treated with 50 mM DTT or 4-DPS (180–650 µM) in SEM buffer for 5 min on ice, respectively. To terminate the redox reaction, samples were supplemented with 50 mM iodoacetamide and incubated on ice for 10 min. The proteins were separated by reducing or non-reducing SDS–PAGE followed by western blotting.

Article

In vivo photocrosslinking

In vivo BPA crosslinking was performed as described previously[4]. For BPA crosslinking of Tom22, TSY1/pTS1-X (X: 132, 136 and 140) cells[24] were grown in 5 ml of SD (−Trp, −Leu) for 36 h at 30 °C. The cells were collected by centrifugation (1,500g, 5 min, 25 °C), resuspended in 50 ml of SGal (−Trp, −Leu, +1 mM BPA) and cultured for 18 h at 30 °C. Half of the culture was irradiated by UV (365 nm) for 7 min, and the other half kept in the dark. Then, the cells were collected by centrifugation (1,500g, 5 min, 4 °C), and Tom22–His$_{10}$ was purified with Ni-NTA (see below). For BPA crosslinking of Tom40, TSY5/pTS6-X (X: 34, 44, 372, 375, 379, 383 and 387) cells[4] were grown in SCGal (−Ura, −Trp) for 48 h at 30 °C, then diluted tenfold in SCD (−Ura, −Trp, +1 mM BPA), and cultured for 22 h at 30 °C. Then the culture was subjected to crosslinking by UV irradiation as in the case of Tom22.

For Ni-NTA purification of the crosslinked products, cells with and without UV irradiation were resuspended in TE buffer (10 mM Tris-HCl pH 8.0 and 1 mM EDTA), treated with 300 mM NaOH, 7% (v/v) 2-mercaptoethanol for 5 min on ice, and then received 10% trichloroacetic acid. The precipitated proteins were washed with ice-cold acetone after centrifugation (20,000g, 10 min, 4 °C), and then solubilized with 1% SDS buffer (40 mM Tris-HCl pH 8.0, 150 mM NaCl, 1% (w/v) SDS, 1 mM PMSF) for 5 min at 60 °C. Insoluble materials were removed by centrifugation (20,000g, 10 min, 25 °C), and the supernatant was diluted fivefold with 0.5% TX-100 buffer (0.5% (v/v) Triton X-100, 50 mM Tris-HCl pH 8.0, 150 mM NaCl, 40 mM imidazole) and incubated for 2 h at 4 °C with Ni-NTA agarose resin. Ni-NTA resin was washed with 0.5% TX-100 buffer 4 times, and bound proteins were eluted by elution buffer (0.5% (v/v) Triton X-100, 50 mM Tris-HCl pH 8.0, 150 mM NaCl, 400 mM imidazole). Eluted proteins were mixed with 0.03% (w/v) sodium deoxycholate and 10% trichloroacetic acid, and kept on ice for 20 min. The precipitated proteins were washed with ice-cold acetone after centrifugation (20,000g, 10 min, 4 °C), then solubilized with 1% SDS buffer for 5 min at 60 °C and subjected to SDS−PAGE followed by western blotting.

Analysis of gel-separated proteins

Radiolabelled proteins were separated by blue native electrophoresis or SDS−PAGE and analysed by autoradiography using Typhoon FLA 7000 phosphoimager and Fuji FLA 9000 phosphoimager. Non-radiolabelled proteins were detected by western blotting. Antibodies were used that had been generated in rabbits against proteins of *S. cerevisiae* by injection of peptides (Cit1, Cyc1, Por1, Rip1, Tim13, Tim23, Tim50, Tom5, Tom40, Tom70) and recombinant full-length or truncated proteins (Mia40, Tom22, Tom40, Sam50, Tim50). The sera were used for western blotting with 1:250 to 1:5,000 dilution. Detection was performed using chemiluminescence, X-ray films or LAS 3000/4000 (FujiFilm). The figure legends indicate how many times the experiments were performed (independent experiments with similar set-ups and results). Data were processed using ImageJ, MultiGauge, Adobe Photoshop and Illustrator CS5, CS6 and CC 2017. Adjustments of brightness and contrast were applied to whole images in linear settings. Uncropped gels and source data are shown in Supplementary Fig. 2.

Mass spectrometry analysis

For matrix-assisted laser desorption/ionization–time-of-flight mass spectrometry (MALDI−TOF-MS) analysis, the purified TOM complex solution was desalted by ZipTip C18 (Merck) and mixed 1:10 with matrix solution (10 mg ml^{-1} α-cyano-4-hydroxycinnamic acid in 0.1% trifluoroacetic acid and 80% acetonitrile). The mixture was then applied onto a target plate (MTP 384 target plate ground steel BC, Bruker), and MS spectra were measured with an autoflex speed MS spectrometer (Bruker) in a positive ion mode protocol. The acquired spectra were analysed with flexAnalysis 3.4 (Bruker). For nano liquid chromatography−tandem mass spectrometry (LC-MS/MS) analysis, the purified

TOM complex was separated by SDS−PAGE, and small TOM proteins (~10 kDa) were extracted from a gel stained with Coomassie brilliant blue and were in-gel digested by trypsin. The peptides were subjected to nanoLC-MS/MS analysis and proteins were identified by Mascot search (Japan Proteomics).

Patch analysis, multiple alignment and conservation analysis

Analyses of basic, acidic and hydrophobic patches were performed using Patch Analyzer in MOE 2015.10 software. The multiple alignments in this paper were generated by MAFFT[61] and displayed using Jalview[62]. The TOM complex evolved independently into various complex forms in eukaryotic lineages[20]. In Opisthokonta (fungi and metazoan) the TOM complex probably maintains the same forms as the yeast TOM complex[20]. For conservation analysis, homologous sequences of TOM complex subunits were obtained from reference proteomes belonging to Opisthokonta using HMMER 3.2.1 (http://hmmer.org); 260, 281, 162, 117 and 100 sequences for Tom40, Tom22, Tom7, Tom6 and Tom5, respectively. The multiple alignments were generated by MAFFT[61] and conservation score are analysed using ConSurf[63].

Reporting summary

Further information on research design is available in the Nature Research Reporting Summary linked to this paper.

Data availability

The cryo-EM density maps have been deposited in the Electron Microscopy Data Bank under accession code EMD-9851. The atomic coordinates have been deposited in the Protein Data Bank under accession code 6JNF. All the data from this study are available in the Article, its Extended Data and Supplementary Information. The uncropped blots, gels and plates are provided in Supplementary Fig. 2.

47. Zheng, W. et al. Adaptive optics improves multiphoton super-resolution imaging. *Nat. Methods* **14**, 869–872 (2017).
48. Rohou, A. & Grigorieff, N. CTFFIND4: Fast and accurate defocus estimation from electron micrographs. *J. Struct. Biol.* **192**, 216–221 (2015).
49. Zivanov, J. et al. New tools for automated high-resolution cryo-EM structure determination in RELION-3. *eLife* **7**, e42166 (2018).
50. Emsley, P., Lohkamp, B., Scott, W. G. & Cowtan, K. Features and development of Coot. *Acta Crystallogr. D* **66**, 486–501 (2010).
51. Adams, P. D. et al. PHENIX: a comprehensive Python-based system for macromolecular structure solution. *Acta Crystallogr. D* **66**, 213–221 (2010).
52. Pettersen, E. F. et al. UCSF Chimera—a visualization system for exploratory research and analysis. *J. Comput. Chem.* **25**, 1605–1612 (2004).
53. Sikorski, R. S. & Hieter, P. A system of shuttle vectors and yeast host strains designed for efficient manipulation of DNA in Saccharomyces cerevisiae. *Genetics* **122**, 19–27 (1989).
54. Model, K. et al. Multistep assembly of the protein import channel of the mitochondrial outer membrane. *Nat. Struct. Biol.* **8**, 361–370 (2001).
55. Opaliński, Ł. et al. Recruitment of cytosolic J-proteins by TOM receptors promotes mitochondrial protein biogenesis. *Cell Rep.* **25**, 2036–2043 (2018).
56. Qiu, J. et al. Coupling of mitochondrial import and export translocases by receptor-mediated supercomplex formation. *Cell* **154**, 596–608 (2013).
57. Ando, T., Uchihashi, T. & Fukuma, T. High-speed atomic force microscopy for nano-visualization of dynamic biomolecular processes. *Prog. Surf. Sci.* **83**, 337–437 (2008).
58. Uchihashi, T., Kodera, N. & Ando, T. Guide to video recording of structure dynamics and dynamic processes of proteins by high-speed atomic force microscopy. *Nat. Protoc.* **7**, 1193–1206 (2012).
59. Milenkovic, D. et al. Identification of the signal directing Tim9 and Tim10 into the intermembrane space of mitochondria. *Mol. Biol. Cell* **20**, 2530–2539 (2009).
60. Thornton, N. et al. Two modular forms of the mitochondrial sorting and assembly machinery are involved in biogenesis of α-helical outer membrane proteins. *J. Mol. Biol.* **396**, 540–549 (2010).
61. Katoh, K. & Standley, D. M. MAFFT multiple sequence alignment software version 7: improvements in performance and usability. *Mol. Biol. Evol.* **30**, 772–780 (2013).
62. Waterhouse, A. M., Procter, J. B., Martin, D. M. A., Clamp, M. & Barton, G. J. Jalview Version 2—a multiple sequence alignment editor and analysis workbench. *Bioinformatics* **25**, 1189–1191 (2009).
63. Ashkenazy, H. et al. ConSurf 2016: an improved methodology to estimate and visualize evolutionary conservation in macromolecules. *Nucleic Acids Res.* **44**, W344–W350 (2016).

Additional information
**Supplementary information** is available for this paper at https://doi.org/10.1038/s41586-019-1680-7.
Correspondence and requests for materials should be addressed to T.E.
**Reprints and permissions information** is available at http://www.nature.com/reprints.
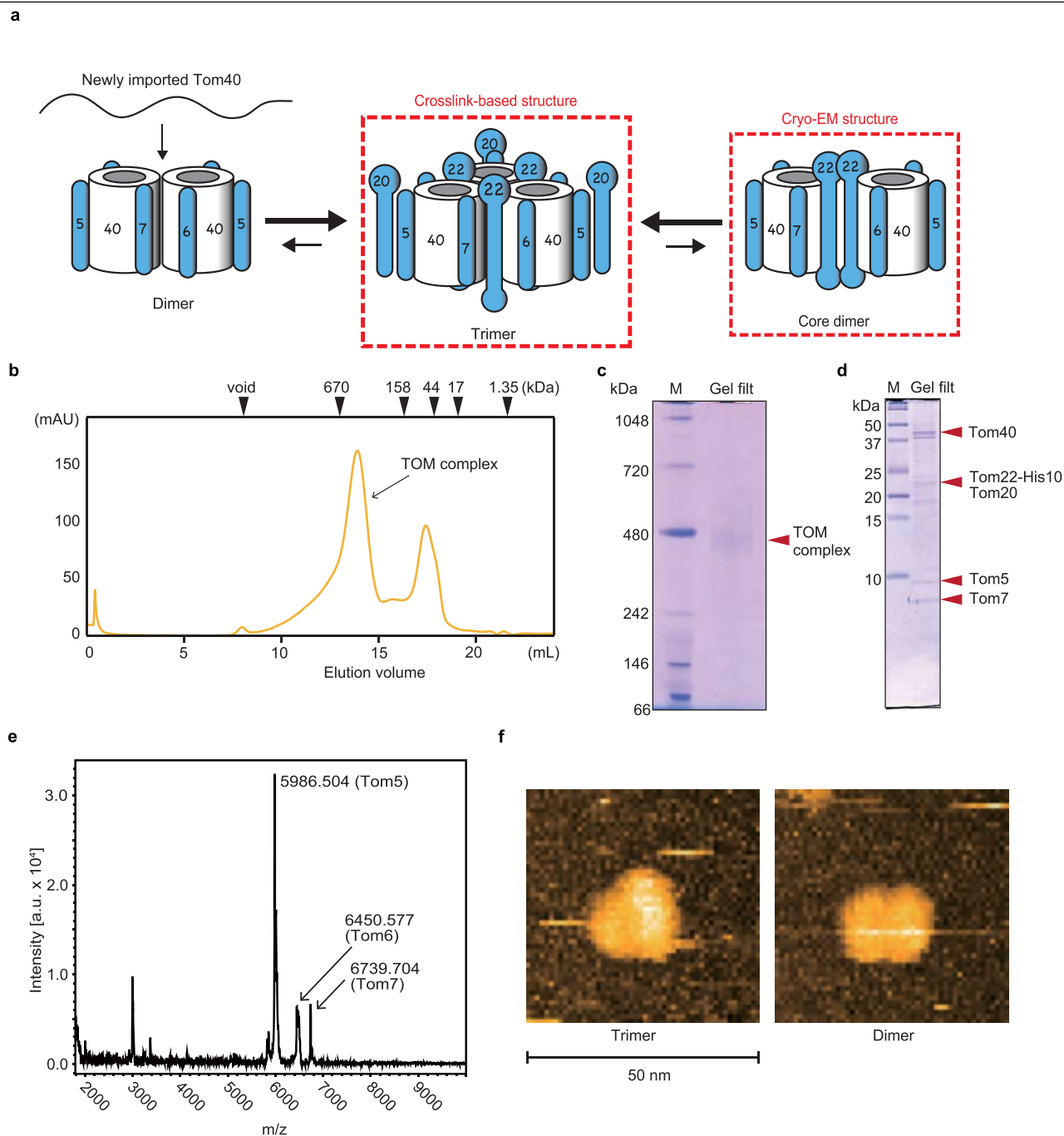
Extended Data Fig. 1 | Purification of the TOM complex. a, Forms of the TOM complex. Newly imported Tom40 takes a β-barrel structure and forms an assembly 'dimer' lacking Tom22 and Tom20. The dimer is matured into the 'trimer' with the receptors Tom22 and Tom20[4]. Even after the maturation, the trimer dynamically exchanges with a minor population of the assembly dimer[4]. After solubilization of mitochondria, the TOM complex can be found as a trimer, containing Tom20 at least partly. Our previous in vivo crosslinking analyses revealed the subunit arrangement of the trimer[4,32], and the present study revealed the high-resolution cryo-EM structure of the dimeric TOM core complex that contains Tom22, but lacks Tom20. **b**, Elution profile of gel filtration of the purified TOM complex. **c**, Blue native electrophoresis gel of the TOM complex stained with Coomassie brilliant blue. The apparent molecular weight of the TOM complex is ~440 kDa on blue native electrophoresis, which corresponds to the trimer. **d**, SDS–PAGE gel of the TOM complex stained with Coomassie brilliant blue. The bands for Tom40, Tom22–His10, Tom20 and Tom5 were assigned by western blotting with antibodies against each subunits. The presence of Tom5, Tom6 and Tom7 were confirmed by mass spectrometry (MS) analyses. The bands for Tom5 and Tom7 were assigned by MS/MS analyses of the tryptic fragments of the proteins contained in each band. **e**, MALDI–TOF MS of purified TOM complex in the m/z range below 10,000. Calculated molecular weights of yeast small TOM subunits are 5986.0 (Tom5), 6407.6 (Tom6), and 6871.0 (Tom7). Tom7 appears to lack the N-terminal Met, and Tom6 may be acetylated. The data are representative of six (**b**, **c**), four (**d**) and two (**e**) independent experiments. **f**, Typically observed particles of HS-AFM images of the TOM complex trimer and dimer on mica.
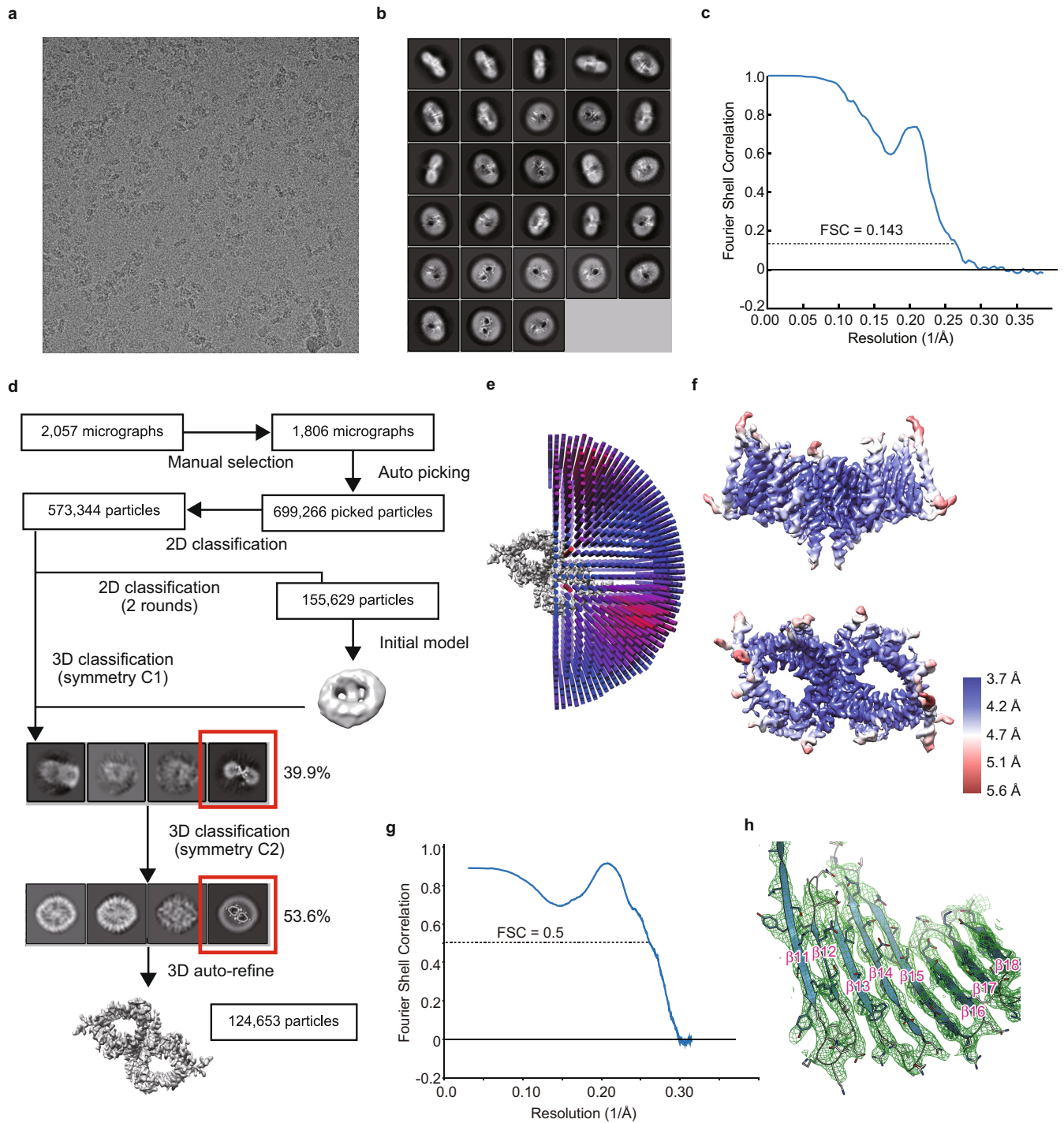
Extended Data Fig. 2 | Cryo-EM analysis of the TOM complex. a, A micrograph of the TOM complex. **b**, Selected 2D classes showing various orientations. **c**, FSC curve after the application of soft mask in RELION, showing FSC of 0.143. **d**, The schematic workflow of the steps followed in data processing leading to the final structure of the TOM core complex. **e**, Angular particle distribution in the final reconstruction. **f**, Local map resolution of the final TOM complex structure with colours according to the scale on the right side. **g**, FSC curve between the EM map and the atomic model of the TOM complex. **h**, An example of the fit of the model into the density map; the region around β-strands 11–18 of Tom40 is shown.
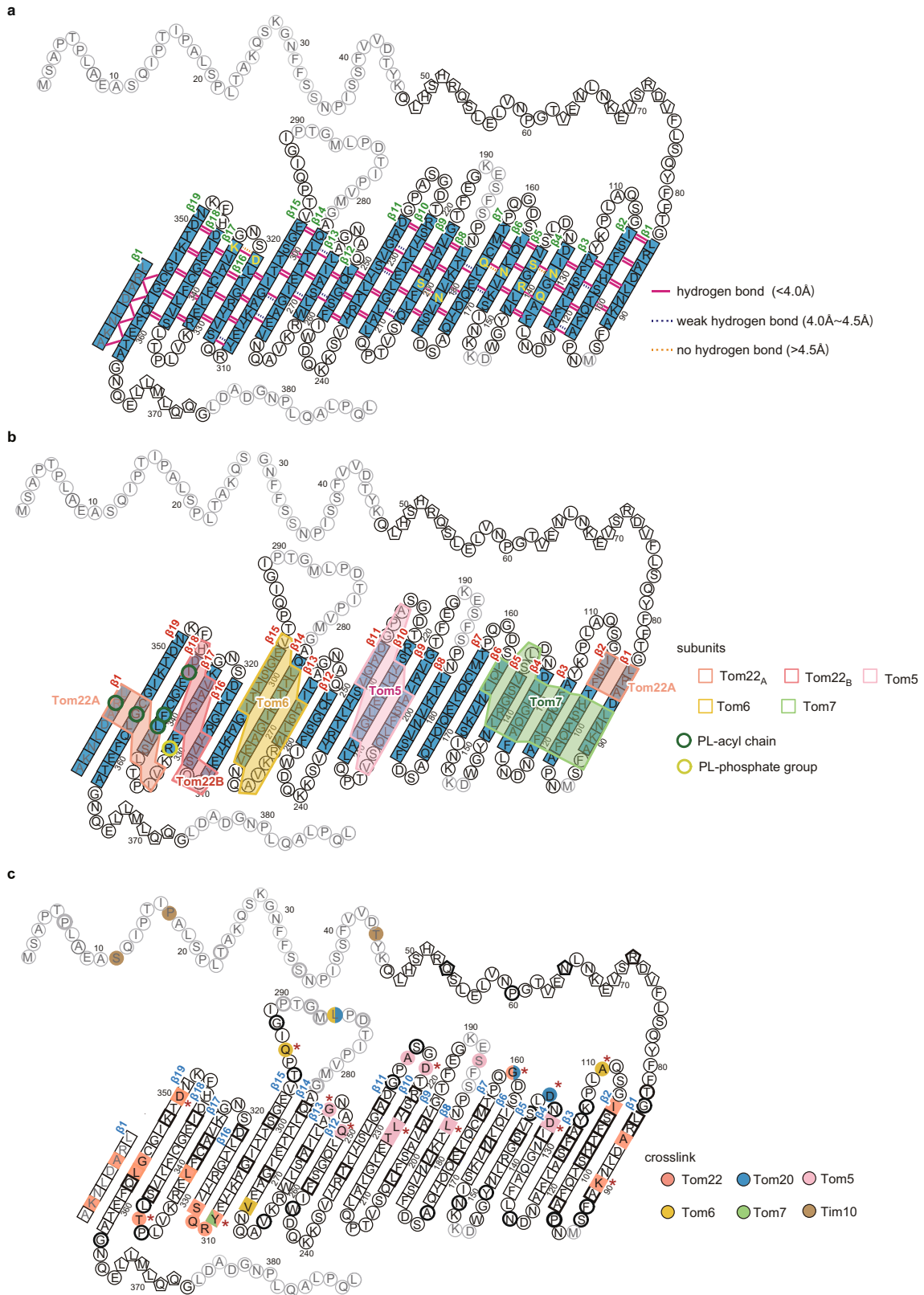
Extended Data Fig. 3 | β-barrel structure of Tom40. a, Hydrogen bonds between the 19 β-strands on the basis of the EM structure. Circles, pentagons and squares indicate residues in loops, α-helices and β-strands, respectively. Disordered regions are coloured in grey. Hydrogen bond, CO–NH distance < 4.0 Å; weak hydrogen bond, 4.0 Å ≤ CO–NH distance ≤ 4.5 Å; no hydrogen bond, 4.5 Å < CO–NH distance. **b**, Relative positions of the other TOM subunits and phospholipid in contact with the Tom40 β-barrel. **c**, Summary of previous crosslinking results of Tom40[4]. BPA-incorporated residues are labelled in bold. Crosslinked partners are indicated by different colours. Residues labelled with a red asterisk are not within a distance of 5 Å from their crosslinked partners in the EM structure.
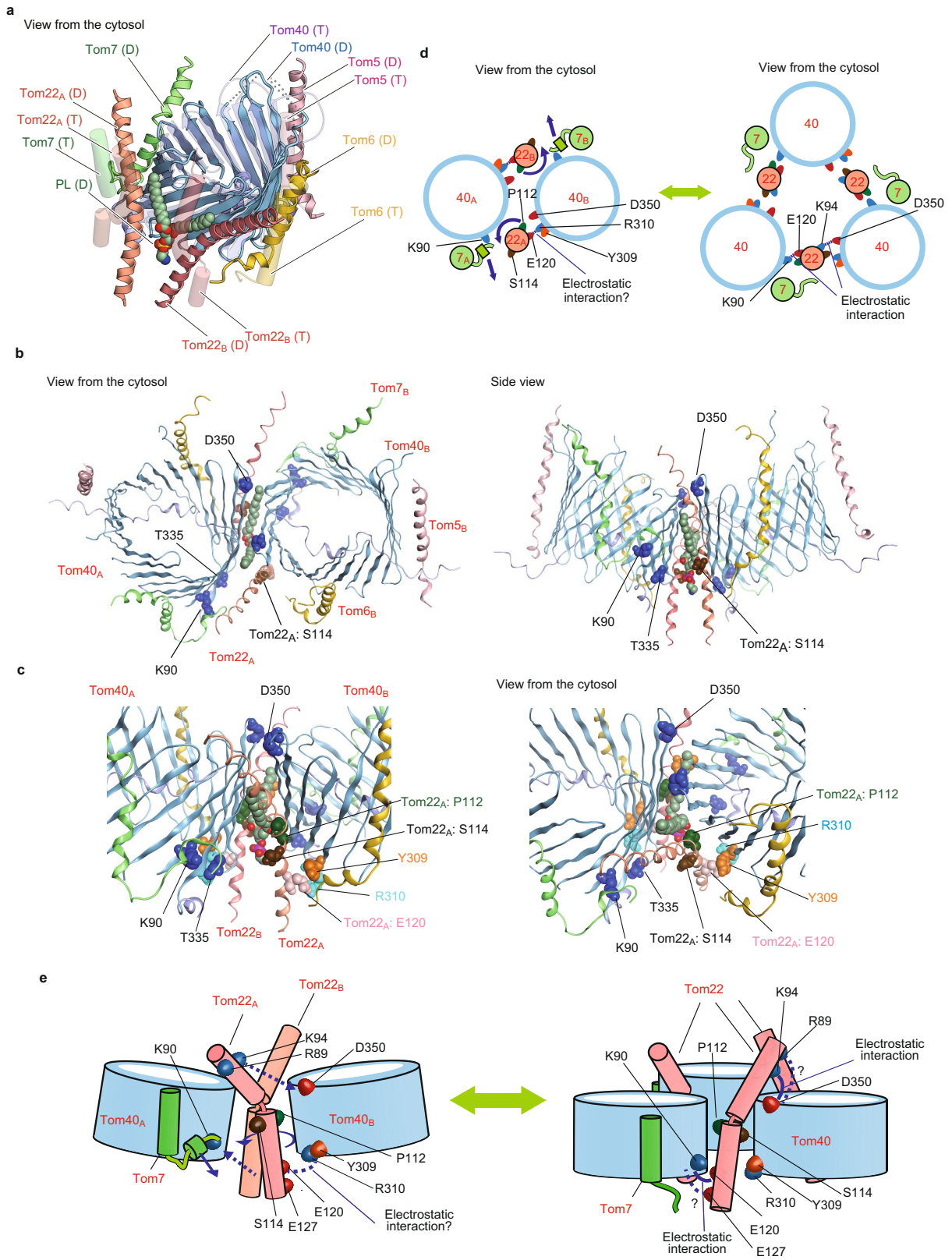
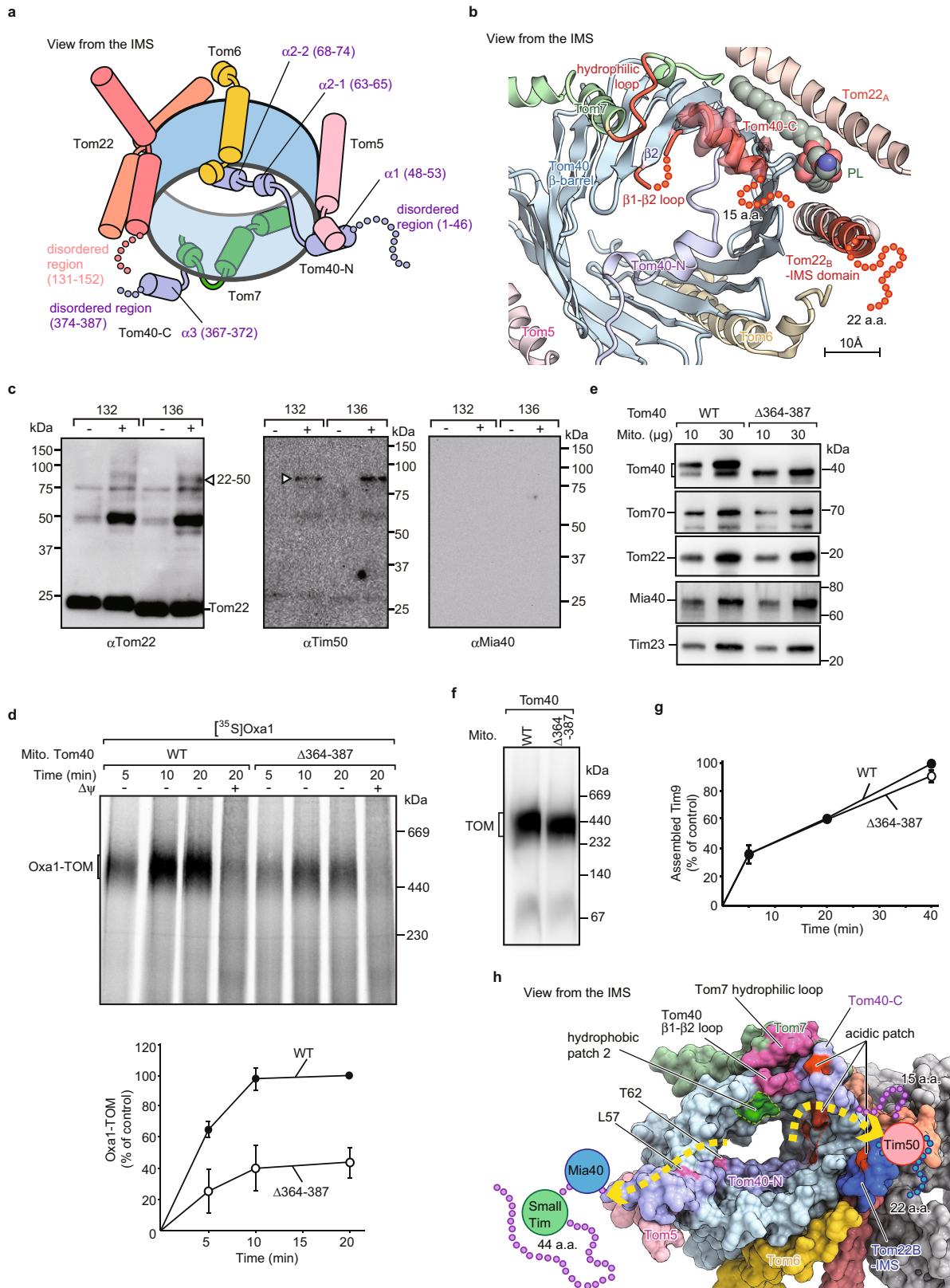**Extended Data Fig. 4** | See next page for caption.

Article

Extended Data Fig. 4 | Model for transition between the Tom22-containing dimer and trimer. a, Comparison of the cryo-EM structure of Tom22-containing dimer (D) and crosslinked-based structure model of Tom22-containing trimer (T). **b**, The residues whose proximity relationships are inconsistent between the trimer (crosslinking) and the dimer (EM structure) are mapped on the EM structure. Top view from the cytosolic side (left) and side view (right) of the EM dimer structure (cartoon model) with the side chains (space-filling model) of the residues that were crosslinked to other subunits[4] but were not within a distance of 4.5 Å from the crosslinked partners in the EM structure (Supplementary Table 1), and therefore judged to be important for formation of the mature trimer[4]. **c**, The residues suggesting the possible difference in the subunit interfaces between the trimer and dimer are mapped on the EM structure. Although $Tom22_A$ P112 and $Tom40_B$ Y309 face each other in the EM structure, the Tom22 transmembrane helix was crosslinked to two Tom40 molecules through Tom22 P112 and Tom40 Y309[4], suggesting that these two residues should not face each other in the trimer. Tom22 E120 and Tom40 R310 are evolutionary conserved (Extended Data Fig. 7 and Supplementary Table 2) and electrostatic interaction between the two residues would contribute to stabilization of the dimer. **d**, **e**, Upon formation of the trimer from the dimer, the Tom22 transmembrane helix in the EM structure may rotate (with a possible conformational change), so that $Tom22_A$ P112 faces the $Tom40_A$ molecule and $Tom22_A$ S114 interacts with the $Tom40_B$ molecule. This rotation would lead to a switch of the electrostatic-interaction pairs from Tom22 E120 and Tom40 R310 to Tom22 E120 and Tom40 K90 with possible concomitant movement of the Tom7 C-terminal segment; the second short C-terminal helix of Tom7 appears to be stabilized by the hydrogen bond between the carbonyl O of L51 in Tom7 and the side-chain NH of K90 in Tom40 in the dimer, which is probably lost in the trimer. The rotation of the Tom22 transmembrane helix would also allow K94 and R89 of Tom22 to interact with D350 of the neighbouring Tom40 molecule. Basic and acidic residues are coloured in blue and red, respectively.
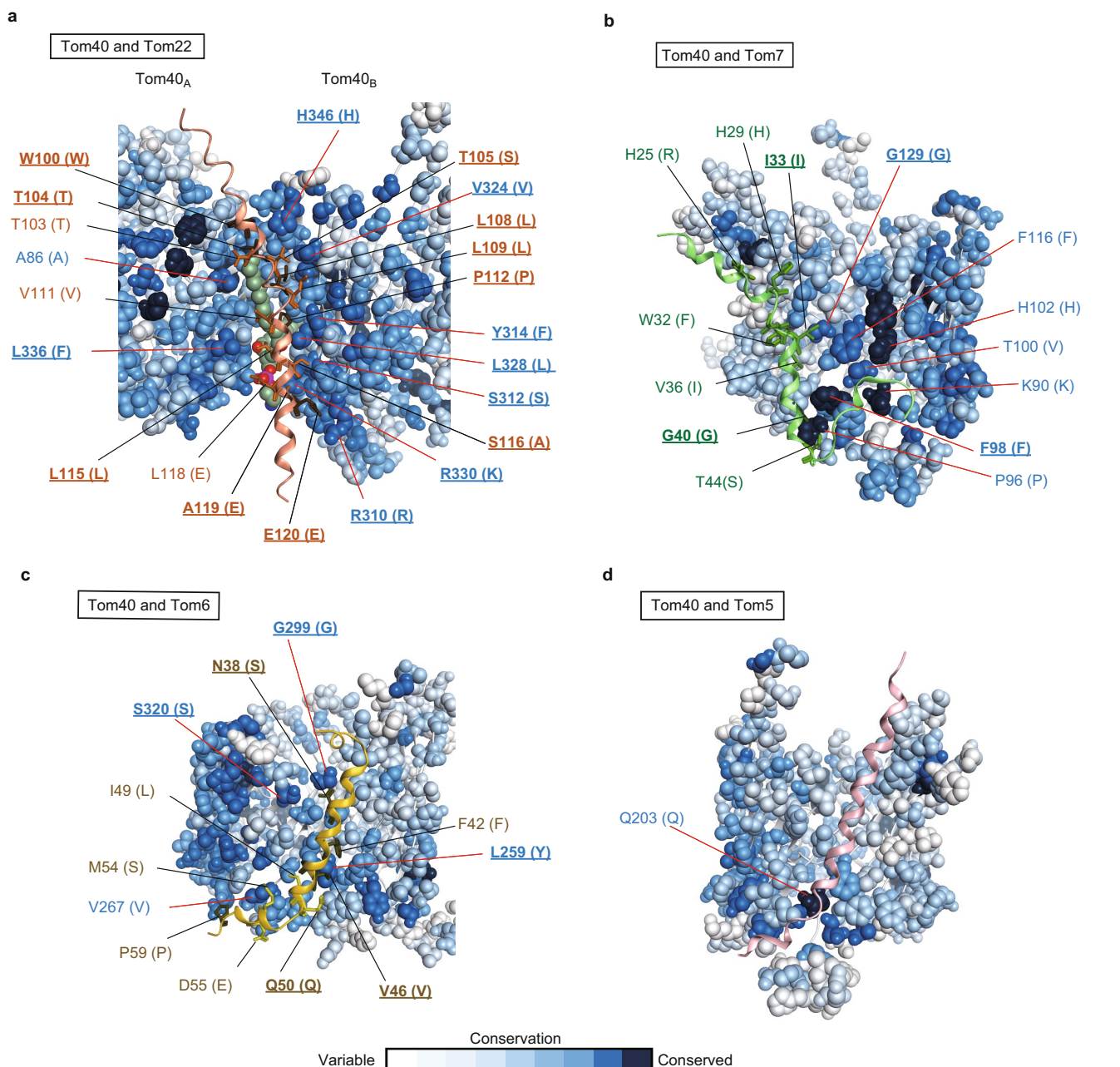
Extended Data Fig. 5 | Conserved interactions between the Tom40 β-barrel and the α-helical subunits. a–**d**, Interactions are shown between the Tom40 β-barrel and the α-helical subunits Tom22 (**a**), Tom7 (**b**), Tom6 (**c**) and Tom5 (**d**). Tom40 residues of the β-barrel outer wall and loops are shown in space-filling form and coloured by evolutionary conservation (darker blue represents more conserved residues). Tom40 residues at 'conserved amino acid' (conserved) positions within 4.5 Å distance of the α-helical subunits are labelled. The main chains of the α-helical subunits are shown in ribbon form, and residues at conserved positions within 4.5 Å distance of Tom40 are shown in stick form, labelled, and coloured by evolutionary conservation (deeper colour represents more highly conserved residues). Residues in parentheses are the most frequently observed residue at each conserved position. Pairs of residues at conserved positions of Tom40 β-barrel and α-helical subunits in proximity (≤4.5 Å) are underlined and bolded: Tom40$_B$ R310 (R) and Tom22 E120 (E),

Tom40$_B$ S312 (S) and Tom22 S116 (A), Tom40$_B$ Y314 (F) and Tom22 L109 (L), Tom40$_B$ V324 (V) and Tom22 L109 (L), Tom40$_B$ V324 (V) and Tom22 L108 (L), Tom40$_B$ V324 (V) and Tom22 T105 (S), Tom40$_B$ L328 (L) and Tom22 P112 (P), Tom40$_B$ R330 (K) and Tom22 A119 (E), Tom40$_A$ L336 (F) and Tom22 L115 (L), Tom40$_B$ H346 (H) and Tom22 T105 (S), Tom40$_B$ H346 (H) and Tom22 T104 (T), and Tom40$_B$ H346 (H) and Tom22 W100 (W) (**a**); Tom40 F98 (F) and Tom7 G40 (G) and Tom40 G129 (G) and Tom7 I33 (I) (**b**); Tom40 L259 (Y) and Tom6 V46 (V), Tom40 L259 (Y) and Tom6 Q50 (Q), Tom40 G299 (G) and Tom6 N38 (S) and Tom40 S320 (S) and Tom6 N38(S) (**c**). No conserved proximate residue pair was found between Tom40 and Tom5 (**d**). Phospholipid (modelled as phosphatidylethanolamine) is shown in space-filling form; carbon, nitrogen, oxygen and phosphorus are coloured light green, blue, red and magenta, respectively (**a**).

a View from the IMS

b View from the IMS

c

d

e

f

g

h View from the IMS

Extended Data Fig. 6 | See next page for caption.

Extended Data Fig. 6 | Formation of the two exit sites of the TOM channel for different classes of precursor proteins. a, Disordered regions of Tom22 and Tom40 facing the IMS. **b**, The TOM complex viewed from the IMS side shows that the *trans* presequence binding site (orange) is formed by the hydrophilic loop of Tom7 (residues 43–49), the hydrophilic β1–β2 loop (residues 92–96, M94 is disordered) and C-terminal domain (residues 363–387, residues after L374 are disordered, G363–E366 form a loop and E367–G373 form a helix) of Tom40 and the acidic IMS domain of Tom22 (residues 120–152, residues after 131 are disordered, the transmembrane helix is extended up to F130). Disordered parts are shown with beads. **c**, Crosslinked products of Tom22 containing BPA at the indicated positions were detected by the indicated antibodies. Crosslinked products between Tom22 and Tim50 (22–50) are indicated. Representative data of two independent experiments. **d**, Radiolabelled Oxa1 precursor was imported into wild-type and Tom40(Δ364–387) mitochondria for the indicated periods in the absence or presence of a membrane potential (Δψ) and analysed by blue native electrophoresis and autoradiography. Representative data of three independent experiments. Quantification of Oxa1 bound to the TOM complex; mean values ± s.e.m. (*n* = 3 biologically independent experiments); the amount of bound Oxa1 in wild-type mitochondria after 20 min (−Δψ) was set as 100%

(control). **e**, Mitochondria isolated from wild-type and Tom40(Δ364–387) yeast grown at 30 °C were analysed by SDS–PAGE and western blotting using the indicated antisera. Representative data of four independent experiments. Amount of total mitochondrial protein is indicated. **f**, Mitochondria isolated from wild-type and Tom40(Δ364–387) yeast grown at 30 °C were analysed by blue native electrophoresis and western blotting with Tom40 antiserum. Representative data of four independent experiments. **g**, Radiolabelled Tim9 was imported and assembled into the TIM22 complex in wild-type and Tom40(Δ364–387) mitochondria; data are mean ± s.e.m. (*n* = 3 biologically independent experiments); the amount in wild-type mitochondria after 40 min import was set as 100% (control). **h**, The *trans* presequence binding sites for presequence-containing proteins (**b**) and the N extension of Tom40 recruiting small TIM chaperones (for presequence-lacking β-barrel and carrier proteins) and Mia40 (for MIA substrates) are spatially separated to form distinct precursor exit sites at the outlet of the TOM channel. The two exit sites are connected to the different translocation paths (yellow broken lines) that include either the aligned acidic patches (red) or the aligned hydrophobic patches (green) inside the Tom40 β-barrel pore (Extended Data Fig. 9). Disordered parts are shown with beads.
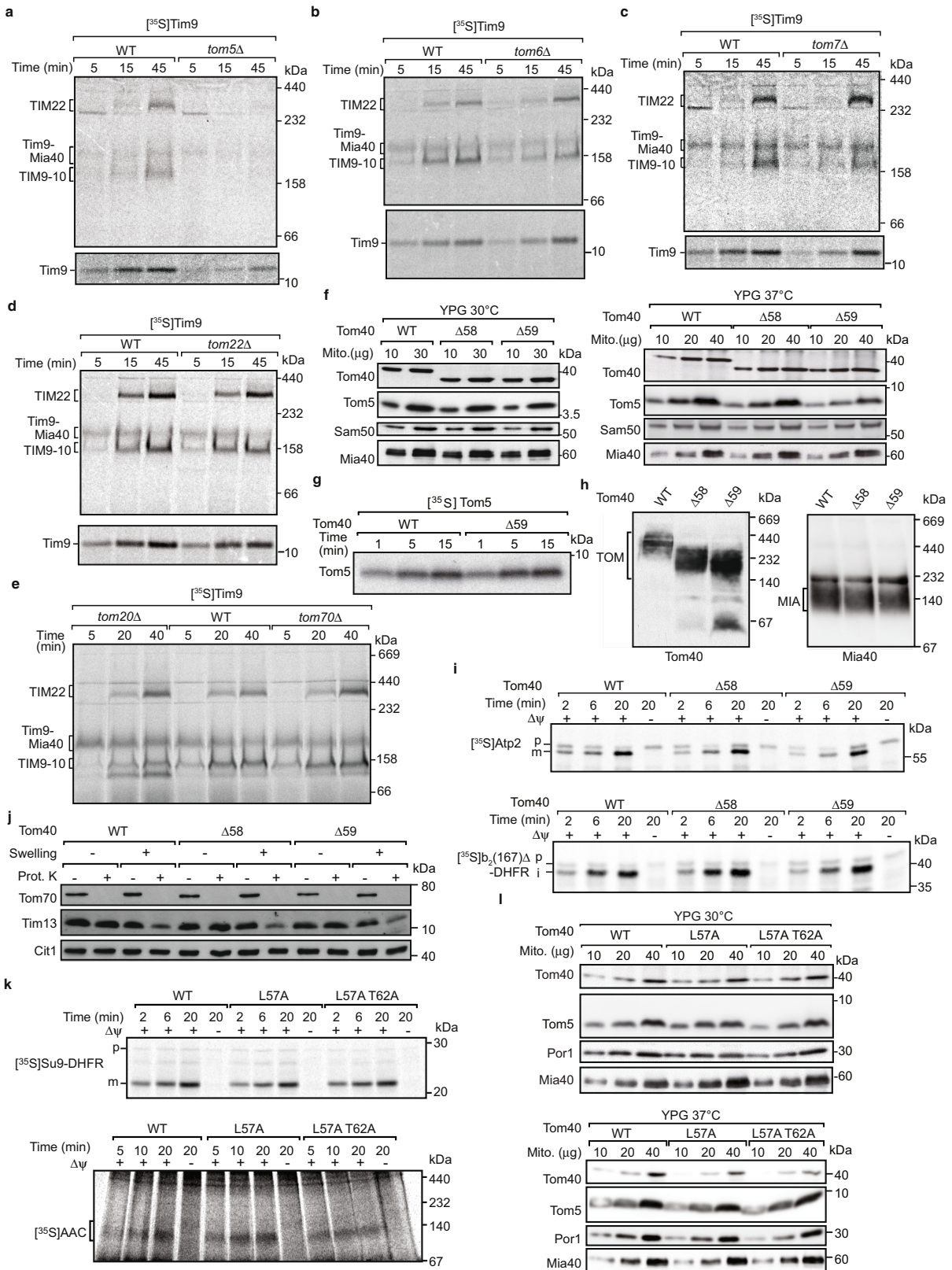
Extended Data Fig. 7 | See next page for caption.

Extended Data Fig. 7 | Roles of Tom5 and the N extension of Tom40 in MIA import and assembly. a–e, Import of radiolabelled Tim9 precursor into isolated wild-type, *tom5Δ*, *tom6Δ*, *tom7Δ*, *tom22Δ*, *tom20Δ* and *tom70Δ* mitochondria, analysed by blue native electrophoresis (top) and SDS–PAGE (bottom). TIM22, TIM22 complex; Tim9–Mia40, mixed disulfide intermediate of Tim9 with Mia40; TIM9–10, Tim9–Tim10 complex. Representative data of three (**a**, **b**, top), four (**d**, top) or two (other panels) independent experiments. **f**, Mitochondria were isolated from wild-type, Tom40(Δ58) and Tom40(Δ59) yeast cells, which were grown at 30 °C and, where indicated, additionally shifted to 37 °C for 12 h, and analysed by SDS–PAGE and western blotting using the indicated antisera. Representative data of two independent experiments. **g**, Radiolabelled Tom5 precursor was imported into mitochondria isolated from wild-type and Tom40(Δ59) yeast cells, which were grown at 30 °C and shifted to 37 °C for 12 h, followed by incubation with sodium carbonate. The carbonate-resistant pellets were analysed by SDS–PAGE and autoradiography. Representative data of three independent experiments. **h**, Mitochondria of wild-type, Tom40(Δ58) and Tom40(Δ59) cells grown at 30 °C were analysed by blue native electrophoresis and western blotting using Tom40- and Mia40-specific antisera. Representative data of two independent experiments. **i**, Imports of radiolabelled Atp2 and $b_2(167)\Delta$DHFR into wild-type, Tom40(Δ58) and Tom40(Δ59) mitochondria were analysed by SDS–PAGE. Representative data of three independent experiments. $\Delta\psi$, membrane potential; p, precursor form; m, mature form; i, intermediate form. **j**, Mitochondria of wild-type, Tom40(Δ58) and Tom40(Δ59) cells grown at 30 °C were subjected to hypo-osmotic swelling and treatment with proteinase K (Prot. K) as indicated. Proteins were analysed by SDS–PAGE and western blotting using the indicated antisera. Representative data of two independent experiments. The IMS protein Tim13 shows that the outer membranes of (non-swollen) Tom40(Δ58) and Tom40(Δ59) mitochondria were intact like those of wild-type mitochondria. **k**, Import of radiolabelled Su9–DHFR precursor (top) or AAC (bottom) into wild-type, Tom40(L57A) and Tom40(L57A/T62A) mitochondria was analysed by SDS–PAGE (top) or blue native gel (bottom). Representative data of three (Su9–DHFR) or two (AAC) independent experiments. **l**, Mitochondria of wild-type, Tom40(L57A) and Tom40(L57A/T62A) strains grown at 30 °C and, where indicated, additionally shifted to 37 °C for 29.5 h, were analysed by SDS–PAGE and western blotting using the indicated antisera. Representative data of two independent experiments.
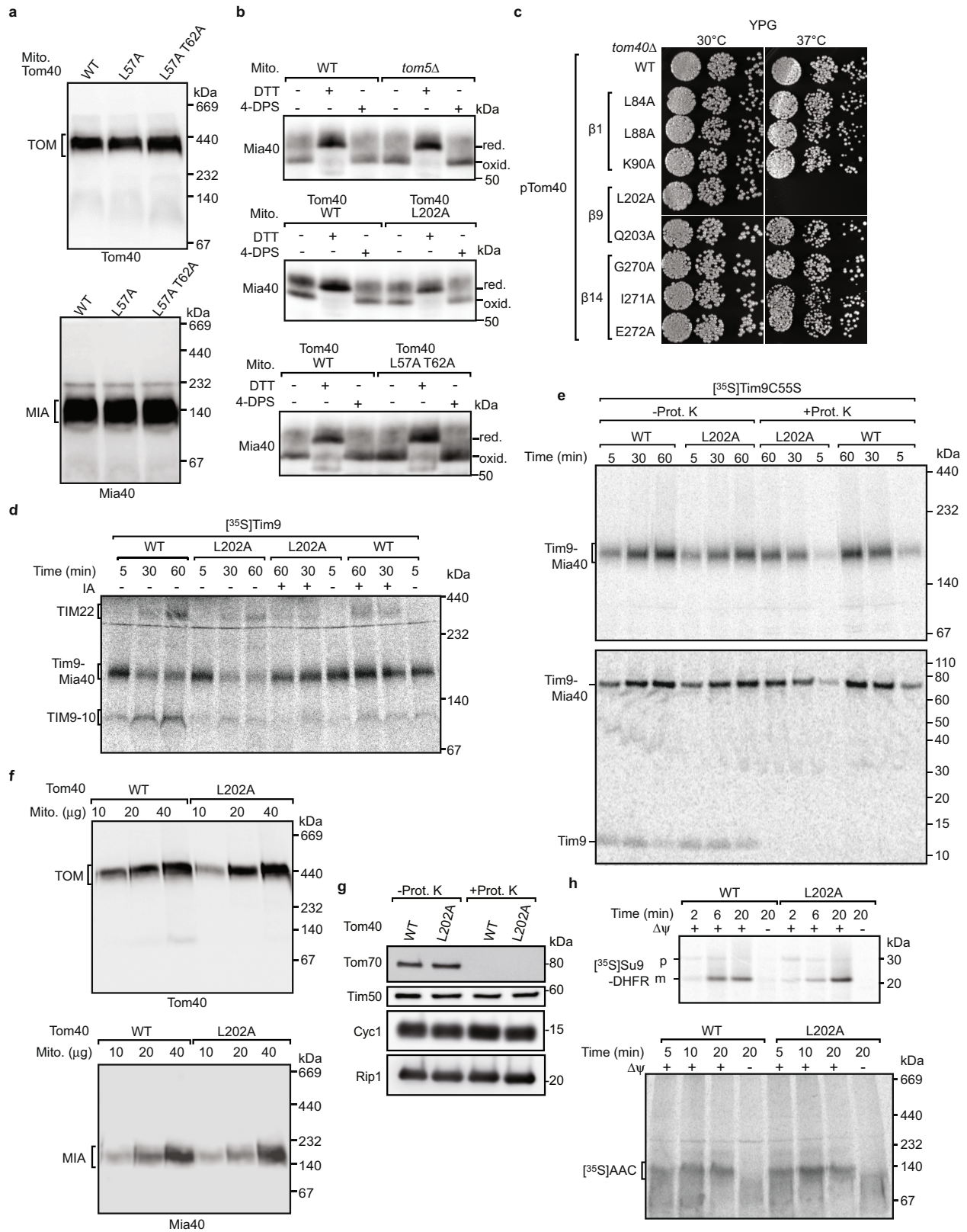
Extended Data Fig. 8 | See next page for caption.

**Extended Data Fig. 8 | MIA import and assembly are disturbed in point mutants of the Tom40 N extension. a**, Wild-type, Tom40(L57A) and Tom40(L57A/T62A) mitochondria from cells grown at 30 °C were analysed by blue native electrophoresis and western blotting using Tom40- and Mia40-specific antisera. Representative data of two independent experiments. **b**, Wild-type, *tom5Δ*, Tom40(L202A) and Tom40(L57A/T62A) mitochondria were treated with DTT or 4-DPS and the redox state of Mia40 was analysed by non-reducing SDS–PAGE and western blotting. Representative data of three independent experiments. Red, reduced form; oxid., oxidized form. **c**, Growth analysis of yeast strains expressing the indicated Tom40 variants on YPG. Representative data of two independent experiments. **d**, Radiolabelled Tim9 was imported into isolated wild-type and Tom40(L202A) mitochondria for 5 min, followed by addition of iodoacetamide (IA), and incubated further as indicated. The import was analysed by blue native electrophoresis. Representative data of two independent experiments. TIM22, TIM22 complex; Tim9–Mia40, mixed disulfide intermediate of Tim9 with Mia40; TIM9–10, Tim9–Tim10 complex. **e**, Import of radiolabelled Tim9(C55S) into wild-type and Tom40(L202A) mitochondria followed by treatment with proteinase K as indicated. The import was analysed by blue native electrophoresis (top) and non-reducing SDS–PAGE (bottom). Representative data of two independent experiments. Tim9–Mia40, mixed disulfide intermediate of Tim9(C55S) with Mia40. **f**, Wild-type and Tom40(L202A) mitochondria from cells grown at 30 °C were analysed by blue native electrophoresis and western blotting using Tom40 and Mia40 specific antisera. Representative data of two independent experiments. **g**, Wild-type and Tom40(L202A) mitochondria from cells grown at 30 °C were treated with proteinase K where indicated. Representative data of two independent experiments. The stability of IMS-exposed proteins indicates that the outer membranes of Tom40(L202A) mitochondria were intact like those of wild-type mitochondria. **h**, Import of radiolabelled Su9–DHFR (top) and AAC (bottom) into wild-type and Tom40(L202A) mitochondria was analysed by SDS–PAGE (top) or blue native electrophoresis (bottom). Representative data of three independent experiments.
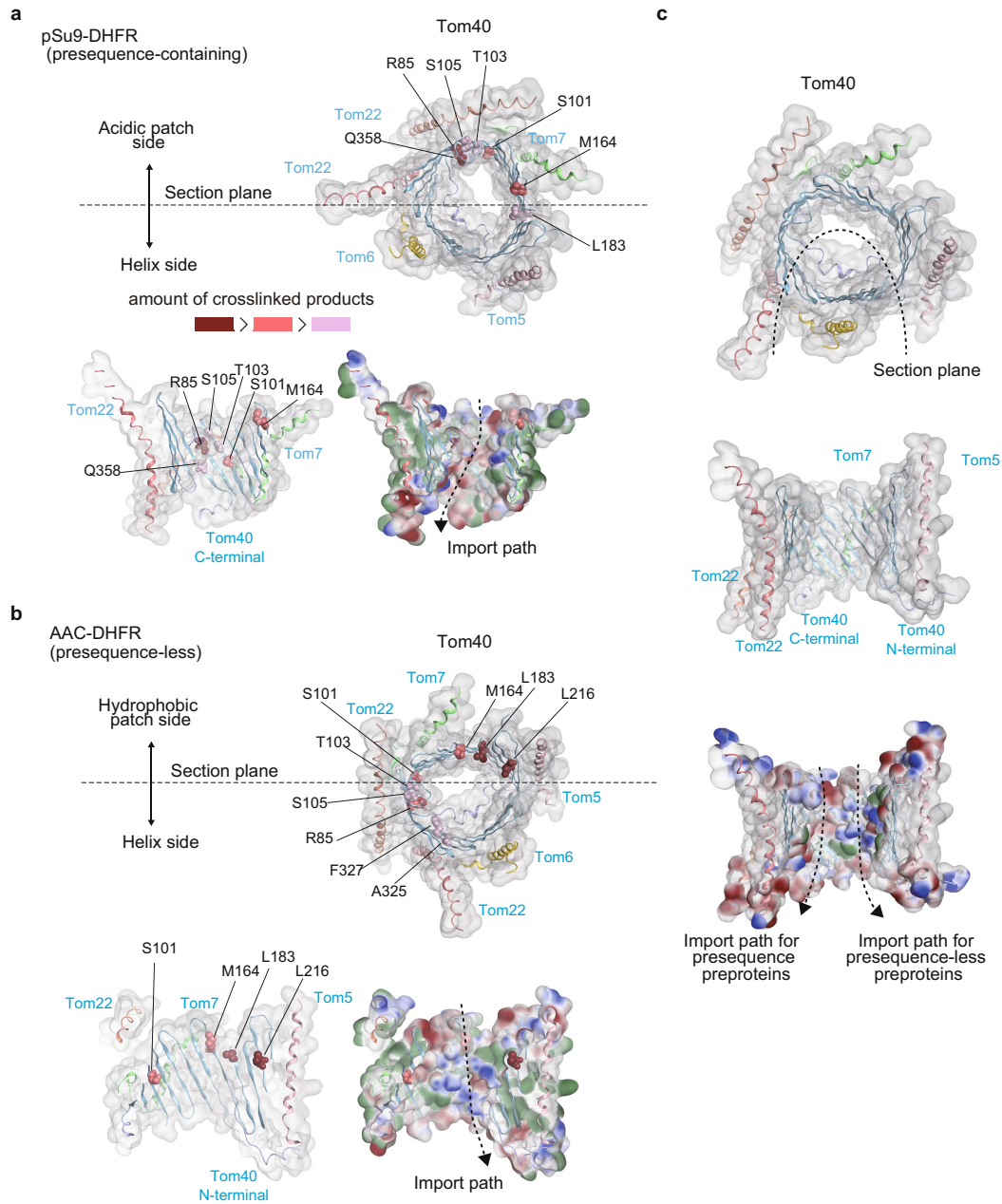
Extended Data Figure 9 | The pore interior of Tom40 and precursor import paths. a, **b**, The views from the cytosol (top) and cut-away views (bottom) for Tom40. Section planes for the cut-away views are indicated with broken lines in the top panels. The side chains of the Tom40 residues crosslinked to the translocation intermediates of a presequence-containing precursor pSu9–DHFR (**a**) and of a hydrophobic presequence-lacking precursor AAC–DHFR (**b**) are shown on the EM structure with colour reflecting the amount of crosslinked products detected[4]. The acidic patches (red) and hydrophobic patches (green) are shown in the cut-away views for the β-barrel side of the pore interior of Tom40. Possible precursor translocation paths are indicated with arrows by broken lines (bottom). **c**, Section curved plane for the cut-away views (centre, bottom) is indicated with a broken line in the view from the cytosolic side (top). The acidic patches (red), hydrophobic patches (green) and possible precursor translocation paths (broken lines) are shown (bottom).

Extended Data Table 1 | Cryo-EM data collection, refinement and validation statistics

	ScTOM complex (EMDB-9851) (PDB 6JNF)
Data collection and processing	
Magnification	96,000
Voltage (kV)	300
Electron exposure (e–/Å^2)	50
Defocus range (μm)	-0.5 – -3.0
Pixel size (Å)	0.861
Symmetry imposed	C2
Initial particle images (no.)	699,268
Final particle images (no.)	124,653
Map resolution (Å) FSC threshold	3.81 0.143
Map resolution range (Å)	3.6 – 5.7
Refinement	
Initial model used (PDB code)	5O8O
Model resolution (Å) FSC threshold	3.82 0.5
Model resolution range (Å)	3.6 – 5.7
Map sharpening B factor (Å^2)	-102.164
Model composition Non-hydrogen atoms Protein residues Ligands	7,271 924 1
B factors (Å^2) Protein Ligand	89.75 38.29
R.m.s. deviations Bond lengths (Å) Bond angles (°)	0.008 1.178
Validation MolProbity score Clashscore Poor rotamers (%)	1.96 4.96 1.02
Ramachandran plot Favored (%) Allowed (%) Disallowed (%)	83.33 16.67 0.00

nature research

Corresponding author(s):   Toshiya Endo

Last updated by author(s):   2019/09/23

Reporting Summary

Nature Research wishes to improve the reproducibility of the work that we publish. This form provides structure for consistency and transparency in reporting. For further information on Nature Research policies, see Authors & Referees and the Editorial Policy Checklist.

Statistics

For all statistical analyses, confirm that the following items are present in the figure legend, table legend, main text, or Methods section.

n/a	Confirmed	
☐	☒	The exact sample size (*n*) for each experimental group/condition, given as a discrete number and unit of measurement
☐	☒	A statement on whether measurements were taken from distinct samples or whether the same sample was measured repeatedly
☒	☐	The statistical test(s) used AND whether they are one- or two-sided *Only common tests should be described solely by name; describe more complex techniques in the Methods section.*
☒	☐	A description of all covariates tested
☒	☐	A description of any assumptions or corrections, such as tests of normality and adjustment for multiple comparisons
☐	☒	A full description of the statistical parameters including central tendency (e.g. means) or other basic estimates (e.g. regression coefficient) AND variation (e.g. standard deviation) or associated estimates of uncertainty (e.g. confidence intervals)
☒	☐	For null hypothesis testing, the test statistic (e.g. *F*, *t*, *r*) with confidence intervals, effect sizes, degrees of freedom and *P* value noted *Give P values as exact values whenever suitable.*
☒	☐	For Bayesian analysis, information on the choice of priors and Markov chain Monte Carlo settings
☒	☐	For hierarchical and complex designs, identification of the appropriate level for tests and full reporting of outcomes
☒	☐	Estimates of effect sizes (e.g. Cohen's *d*, Pearson's *r*), indicating how they were calculated

Our web collection on statistics for biologists contains articles on many of the points above.

Software and code

Policy information about availability of computer code

Data collection	EPU 1.11.1.50 was used for cryo-EM data collection. Data collection of gel-separated proteins are described in Methods section.
Data analysis	Data processing for cryo-EM and single particle analyses, RELION-3.0, MotionCor2_1.1.0, CTFFIND-4.1.13, and EMAN2.2 were used. Coot 0.8.9.1 was used for model building, and Phenix version 1.14-3260 was used for refinement for the structural determination of the TOM complex. Molecular Operating Environment (MOE) 2 2015.10 (commercial software) was used for patch analysis, MAFFT version 7.419 (open software) and Jalview 2.10.5 (open software) for multiple alignment. MOE version 2016.08 (commercial software), CueMol2 version 2.2.3.443, and UCSF Chimera version 1.13.1 were used for structural analyses and presentation. consurf (web server (http://consurf.tau.ac.il/)), HMMER version 3.2.1 (web server (http://hmmer.org)) and MAFFT version 7.419 (open software) were used for conservation analysis. Data analysis of gel-separated proteins are described in Methods section. Data were processed using ImageJ, MultiGauge, Adobe Photoshop and Illustrator CS5, CS6 and CC 2017.

For manuscripts utilizing custom algorithms or software that are central to the research but not yet described in published literature, software must be made available to editors/reviewers. We strongly encourage code deposition in a community repository (e.g. GitHub). See the Nature Research guidelines for submitting code & software for further information.

Data

Policy information about availability of data

All manuscripts must include a data availability statement. This statement should provide the following information, where applicable:

- Accession codes, unique identifiers, or web links for publicly available datasets
- A list of figures that have associated raw data
- A description of any restrictions on data availability

The cryo-EM density maps have been deposited in the Electron Microscopy Data Bank under accession code EMD-9851. The atomic coordinates have been deposited in the Protein Data Bank under accession code 6JNF.

Field-specific reporting

Please select the one below that is the best fit for your research. If you are not sure, read the appropriate sections before making your selection.

☒ Life sciences ☐ Behavioural & social sciences ☐ Ecological, evolutionary & environmental sciences

For a reference copy of the document with all sections, see nature.com/documents/nr-reporting-summary-flat.pdf

Life sciences study design

All studies must disclose on these points even when the disclosure is negative.

Sample size	Samples size was chosen without the use of statistical measures. The amount of mitochondrial and cellular proteins used for the biochemical assays was chosen based on previous experiences with this specific type of experiments and commonly used sample sizes in the field of research. For key experiments, several test runs were performed to determine the optimal sample size used.
Data exclusions	All relevant data shown. No data were excluded from this study.
Replication	All experiments of this study have been reproduced using the same experimental set-up (amount of cell extracts, mitochondrial proteins, buffers, detergents, affinity matrices etc.) with similar results. The number of the independent replications is stated in the Figure Legends. For Western blots and autoradiography, representative results are shown. For all shown data, successful replications are available.
Randomization	The clones of the yeast strains were selected randomly.
Blinding	No blinding was performed. The yeast strains have to be verified before isolation of materials for cell biological and biochemical analysis.

Reporting for specific materials, systems and methods

We require information from authors about some types of materials, experimental systems and methods used in many studies. Here, indicate whether each material, system or method listed is relevant to your study. If you are not sure if a list item applies to your research, read the appropriate section before selecting a response.

Materials & experimental systems

n/a	Involved in the study
☐	☒ Antibodies
☐	☒ Eukaryotic cell lines
☒	☐ Palaeontology
☒	☐ Animals and other organisms
☒	☐ Human research participants
☒	☐ Clinical data

Methods

n/a	Involved in the study
☒	☐ ChIP-seq
☒	☐ Flow cytometry
☒	☐ MRI-based neuroimaging

Antibodies

Antibodies used	The primary antibodies used were non-commercial antibodies, which were specifically prepared for the authors' laboratories. Antibodies were generated in rabbits against proteins of S. cerevisiae by injection of coupled synthetic peptides derived from the S. cerevisiae antigen sequences (Cit1, Cyc1, Por1, Rip1, Tim13, Tim23, Tim50, Tom5, Tom40, Tom70) or recombinant full length or truncated proteins (Mia40, Tom22, Tom40, Sam50, Tim50). The sera were used for Western blot immunodecoration with 1:250 to 1:5000 dilution.
Validation	The specificity of primary antisera was directly determined by the laboratories of the authors by SDS-PAGE with Western blot analysis of wild-type yeast cell extracts/mitochondrial preparations in comparison to mutant yeast cell extracts/mitochondria, where the corresponding protein was modified by tagging (leading to a gel size shift; in case of genes essential for yeast cell viability) or deletion strains were used (leading to a lack of the specific Western blot signal; in case of viable yeast mutants).

Eukaryotic cell lines

Policy information about cell lines

Cell line source(s)	All yest strains used in this study are described in Supplementary Information Table 3
Authentication	The yeast strains were selected by several rounds of growth on selection medium. Total cell extracts were prepared and the deletion or tagging of a yeast genes was confirmed by the absence of size shift of the corresponding gene product after Western blotting and immunodetection with the corresponding antisera.

Mycoplasma contamination

Mycoplasma contamination is not a problem for yeast cultures. Therefore, the mycoplasma contamination was not analyzed.

Commonly misidentified lines
(See ICLAC register)

No commonly misidentified line were used.